

Newtonian Periodic Three-Body Orbits with Zero Angular Momentum: Linear Stability and Topological Dependence of the Period

V. Dmitrašinović, Ana Hudomal

*Institute of Physics Belgrade, University of Belgrade, Pregrevica 118, Zemun,
P.O.Box 57, 11080 Beograd, Serbia*

Mitsuru Shibayama

*Department of Applied Mathematics and Physics,
Graduate School of Informatics, Kyoto University,
Yoshida-honmachi, Sakyo-ku, Kyoto 606-8501, Japan*

Ayumu Sugita

*Department of Applied Physics, Osaka City University,
3-3-138 Sugimoto, Sumiyoshi-ku, Osaka 558-8585, Japan*

(Dated: March 21, 2019)

Abstract

We report the results of an extended search for planar Newtonian periodic three-body orbits with vanishing angular momentum, that has led to more than 150 new topologically distinct orbits, which is more than three-fold increase over the previously known ones. Each new orbit defines an infinite family of orbits with non-vanishing angular momenta. We have classified these orbits in ten algebraically defined sequences. This allows one to critically test the recently proposed linear dependence of the periods on the orbits' topologies. Approximate linear dependences exist for each sequence, but their root-mean-square deviations are generally larger than the estimated numerical error. We have studied the linear stability of these orbits, with the result that about 20 orbits in total are linearly stable. Such linearly stable orbits form credible starting points for searches of astronomically observable systems. The “progenitor” of a sequence is the orbit with the shortest period in its sequence: seven distinct orbits are the progenitors of the above ten sequences. Six of the seven progenitors are linearly stable, whereas one is on the borderline of stability. These findings are consistent with the Birkhoff-Lewis theorem, which posits that each linearly stable orbit implies the existence of infinitely many periodic orbits.

PACS numbers: 45.50.Jf, 05.45.-a, 95.10.Ce

I. INTRODUCTION

The Newtonian three-body problem is perhaps the oldest open problem in the natural sciences: it has captured the attention of astronomers, mathematicians and physicists for more than three centuries. Finding new periodic orbits is perhaps the first common goal of these three disciplines. In this paper we present more than 150 new types of numerical periodic solutions with zero angular momentum, of which around 20 are linearly stable, which makes them candidates for astronomical observation.

A typical example of the three-body problem is the Sun-Earth-Moon system, that was first investigated by Newton himself, albeit to no avail. To first approximation this system appears as two weakly coupled Keplerian two-body problems - one describing the Earth-Moon subsystem and another one describing the Earth-Moon composite orbiting around the Sun. The coupling of the two quasi-Keplerian systems turns out to be variable in time and rather strong under certain circumstances (“resonances”), in which case the perturbative approximations fails. Nevertheless, exact periodic three-body solutions do exist and two were found, [1, 2], less than 100 years after Newton’s first attempt. These two solutions do not describe the Sun-Earth-Moon system, however.

The first and perhaps only example (known thus far) of a successful theoretical prediction of a realistic three-body system are the Jupiter trojans, the first specimens of which were observed early in the 20th century. These systems correspond to the Lagrange solution, [1], which dates from the 18th century, but whose existence in astronomy became viable only after studies of its linear stability were conducted by Gascheau, [3], and by Routh, [4] in the 19th century. The Euler solution, [2], cannot be discovered by astronomers, precisely because it is always unstable. The vast majority of optically observed triple stars belong to so-called “hierarchical systems”, however, that are fundamentally (topologically) different from both the Lagrange, [1], and the Euler solution, [2]. Numerical solutions to the Newtonian three-body equations of motion that correspond to “hierarchical systems” were found only in the mid-1970’s, however, by independent, yet coordinated works of three groups of researchers, Refs. [6–12]. That was followed by further substantial theoretical/numerical activity on this subject in the late 1970’s, resulting in the discovery of at least one new type (isosceles triangle) of (linearly stable) periodic orbit, see Refs. [13, 14], that is still waiting for its astronomical observation/corroboration, however.

Perhaps the most comprehensive search for new periodic three-body orbits (with non-vanishing angular momenta) of its era, to our knowledge, was conducted by Davoust and Broucke [14]. Therein around 135 orbits’ data (initial conditions and stability coefficients) were reported, based on “approximately three thousand periodic orbits”, and belonging to “about two dozen families”, defined in terms of Strömberg’s notation, [15]. These authors concluded that: (a) “it is clear that a search for new periodic orbits may go on forever”; (b) “a complete inventory of periodic orbits as in the restricted problem is completely out of reach”, and (c) “that not much new information will be gained by more numerical calculations”. Davoust and Broucke’s conclusion (b) was somewhat premature, as their work preceded Montgomery’s, [34], topological classification of periodic orbits, see Sect. III A, however. A subsequent topological analysis of these 20-odd “families” showed that they all belong to (only) three topologically distinct types/families, *viz.* the Lagrange-Euler one, [1, 2], the Broucke-Hadjidemetriou-Hénon one, [6–12], and the “isosceles” one, [13], and their topological-power satellites (for a definition of the topological-power satellite, see Sect. III A below). The stability coefficients (“indices”) of orbits vary as a functions of the angular momentum and the mass ratios. Indeed, one can view Davoust and Broucke’s paper as a study of bifurcations of various Strömberg-type families of orbits as functions of angular momentum and/or stability indices within three topological families.

In the period from 1982 to 2001 only one new topologically distinct family of orbits was discovered [61] - the celebrated “figure-8”, [16–18], which turned out to be stable only in a very narrow range of mass ratios, [18, 19], and therefore of little interest to practicing astronomers. Over the past five to 10 years, around 45 topologically distinct periodic three-body orbits have been found by numerical means, Refs. [20–24], thus exposing Davoust and Broucke’s conclusion (c), about the futility of further numerical studies, as unfounded.

Here, we wish to draw the attention of observational and theoretical astronomers, as well as of applied mathematicians, to those 45 orbits, as well as to more than 150 new orbits that we present below. Linear stability of these 45 orbits had not been studied systematically, however. We present the stability coefficients (a.k.a. “indices”) of roughly 20 linearly stable (“elliptic”) and marginal orbits. We hope that at least a few of these approximately 20 might be observable among more than 3000 newly discovered extra-Solar planetary systems [45]. As it is difficult to nail down the orbital parameters from the observed data, the topology of the orbit should be used as an unambiguous benchmark: after all, it is the topology,

rather than the kinematical properties, that distinguishes one family of three-body orbits from another. For such a search to be conducted, however, one needs a comprehensive compilation of presently known periodic three-body orbits' data, to compare with. For that purpose, we have formed the web site [25] that contains the initial conditions, as well as other pertinent data regarding periodic three-body orbits known to us at the present time.

On the mathematical side, the newly discovered orbits display an unexpected relation between their (scale-invariant) periods and their topologies, [26, 27]. If true in general, that relation predicts infinitely many new orbits with ever longer periods and new, as yet unobserved topologies. Here we present some general arguments (in the form of the Birkhoff-Lewis theorem), as well as specific numerical evidence (of linear stability of progenitor orbits) in support of the conjecture that the thus far observed, as well as several new regularities, extend to infinity. Thus, we agree with Davoust and Broucke's conclusion (a).

The purpose of the present paper is to:

1. report the numerical discovery of 150 new, topologically distinct, planar periodic three-body orbits with equal masses and zero angular momentum, and show how infinitely many more can be found, albeit with ever-longer periods, and with ever-increasing numerical effort;
2. study their linear stability: there are around 20 linearly stable orbits;
3. classify all periodic three-body orbits into ten sequences - with the topology of orbits being described by a (conjugacy class of a) free group element. Orbits belonging to a particular sequence have free group elements (topologies) with a particular algebraic structure;
4. point out that these ten sequences of orbits display a quasi-linear regularity, Eq. (6), between their scale-invariant periods and topologies;
5. point out that the ten sequences can be traced back to seven "progenitor" orbits, which are linearly stable;
6. offer an explanation of the existence of the above points 4. and 5., in terms of the Birkhoff-Lewis theorem, [28].

The paper is divided into eight Sections. In Sect. II we briefly recount the search methods used in this paper - more detailed accounts can be found in Refs. [21, 29]. In Sect. III we discuss the identification methods for periodic orbits: Montgomery’s topological method together with its intrinsic ambiguities. In Sect. IV we briefly review the previously known periodic orbits. Then in Sect. V, we give a general overview of our new orbits together with their classification in ten sequences. In Sect. VI we discuss the linear stability of our orbits, and in Sect. VII the linear stability of so-called progenitor orbits and its relation to the Birkhoff-Lewis theorem. Finally, in Sect. VIII we summarize our results, draw the conclusions and discuss the future (list open questions). In Appendix A we show the details of the newly found orbits.

II. SEARCH METHODS

For the sake of completeness we shall give a brief review of our search method, following the outlines given in Refs. [20, 21, 29].

A. The return proximity function

The return proximity function $d(\mathbf{X}_0, T_0)$ is defined as the absolute minimum of the “distance” of the instantaneous position in phase space $\mathbf{X}(t) = (\mathbf{r}_1(t), \mathbf{r}_2(t), \mathbf{r}_3(t), \mathbf{p}_1(t), \mathbf{p}_2(t), \mathbf{p}_3(t))$ (where $\mathbf{r}_i(t)$ are the Cartesian coordinates and $\mathbf{p}_i(t)$ velocities of all three bodies ($i = 1, 2, 3$) without removing the center-of-mass motion) from the initial condition $\mathbf{X}_0 = (\mathbf{r}_i(0), \mathbf{p}_i(0))$: $d(\mathbf{X}_0, T_0) = \min_{t \leq T_0} |\mathbf{X}(t) - \mathbf{X}_0|$. Here, the distance

$$|\mathbf{X}(t) - \mathbf{X}_0| = \sqrt{\sum_i^3 [\mathbf{r}_i(t) - \mathbf{r}_i(0)]^2 + \sum_i^3 [\mathbf{p}_i(t) - \mathbf{p}_i(0)]^2} \quad (1)$$

is the Euclidean norm between two 12-vectors in phase space, where T_0 is some pre-determined maximum integration time. We define the return time $\tau(\mathbf{X}_0, T_0)$ as the time at which this minimum is reached. Thus, searching for periodic solutions with a period T smaller than a parameter T_0 is equivalent to finding zeros of the return proximity function in that interval. The initial value of T_0 was taken to be around 100 in our search, which is significantly longer than the period of the previously known figure-eight solution, which equals 6.235 in present units.

We used the Runge-Kutta-Fehlberg algorithm, [30, 31] to find zeros of the return proximity function, but any other adaptive time step integration method can be used. The result of application of this algorithm is the minimum value of d . If d_{\min} is less than some (in principle arbitrary) tolerance, we use it as a candidate for a periodic solution. This tolerance was taken as 10^{-4} in our calculations, but can be reduced to further improve the results. So the value of this tolerance plays the role of an initial filter to select candidate regions in phase space. That value is not the final minimum, because thereafter we apply the gradient descent method, Ref. [20, 29].

B. Three-Body Variables

It is advisable to eliminate all constants of the motion, and thus reduce the number of variables in the proximity function. The two obvious symmetries of the three-body system, *viz.* the translational and the rotational symmetry are used to set the total linear and angular momenta equal to zero. The third such symmetry is scale covariance, which sets the overall size of the system. One way to implement the translational and the rotational symmetry is by changing the three-body variables to relative, Jacobi ones, see below. So, we must introduce the relative three-body coordinates and the shape sphere. We shall use the latter for classifying periodic solutions.

The center-of-mass (CM) two-vector \mathbf{R}_{CM} is defined for arbitrary masses as

$$\mathbf{R}_{\text{CM}} = \frac{m_1 \mathbf{r}_1 + m_2 \mathbf{r}_2 + m_3 \mathbf{r}_3}{\sum_{i=1}^3 m_i}. \quad (2)$$

\mathbf{R}_{CM} is a constant of the motion if the total linear momentum $\mathbf{P} = m_1 \dot{\mathbf{r}}_1 + m_2 \dot{\mathbf{r}}_2 + m_3 \dot{\mathbf{r}}_3$ equals zero. Thus we reduce the number of variables in the proximity function $d(\mathbf{X}_0, T_0)$ from twelve to eight.

The three-body dynamics is simplified by use of the two relative coordinate vectors introduced by Jacobi, [32] (see Fig. 1),

$$\boldsymbol{\rho} = \frac{1}{\sqrt{2}}(\mathbf{r}_1 - \mathbf{r}_2) \text{ and } \boldsymbol{\lambda} = \frac{1}{\sqrt{6}}(\mathbf{r}_1 + \mathbf{r}_2 - 2\mathbf{r}_3). \quad (3)$$

There are three independent scalar three-body variables: λ^2 , ρ^2 , and $\boldsymbol{\rho} \cdot \boldsymbol{\lambda}$. The hyper-radius $R = \sqrt{\rho^2 + \lambda^2}$ characterizes the overall size (“scale”) of the orbit and removes one of the

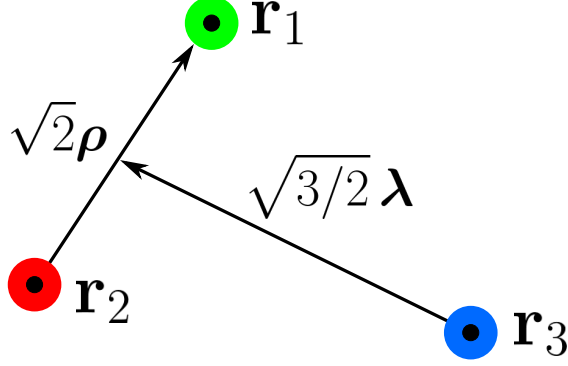


Figure 1: The two three-body Jacobi coordinates ρ, λ .

three scalar variables. It can be always changed to the desired value by means of the scaling rules given below.

We may relate the three scalar variables to the unit three-vector $\hat{\mathbf{n}}$ defined by the Cartesian components

$$\hat{\mathbf{n}} = \left(\frac{2\rho \cdot \lambda}{R^2}, \frac{\lambda^2 - \rho^2}{R^2}, \frac{2(\rho \times \lambda) \cdot \mathbf{e}_z}{R^2} \right). \quad (4)$$

The domain of these three-body variables is a sphere with unit radius, [33, 34], as illustrated in Fig. 2. The sphere coordinates depend only on the shape of the triangle formed by the three bodies, not on R or on its orientation. The equatorial circle corresponds to collinear three-body configurations (degenerate triangles). The three points shown in Fig. 2 correspond to two-body collisions, that are singularities in the potential. Three Euler meridians on the shape sphere, are orthogonal to the equator and pass through one of the collision points and its corresponding Euler point that lies on the equator opposite to the collision point.

We solve the equations of motion using Cartesian coordinates and then use Eq. (4) to graphically represent the solutions. Periodic solutions lead to closed curves on the shape sphere, such as the figure-eight orbit shown in Fig. 2.

Two angles parametrizing the shape sphere together with the hyper-radius R define the three-dimensional configuration space of the planar three-body problem. Thus the nominal dimension of phase space is $6 = 3 + 3$, with the three generalized coordinates describing the configuration space and three conjugate generalized momenta.

Size or energy scaling, $\mathbf{r} \rightarrow \alpha \mathbf{r}$, further reduces the number of dimensions to five, as then the equations of motion imply $t \rightarrow \alpha^{3/2} t$, [36]. Therefore, the velocity scales as $\mathbf{v} \rightarrow \mathbf{v}/\sqrt{\alpha}$,

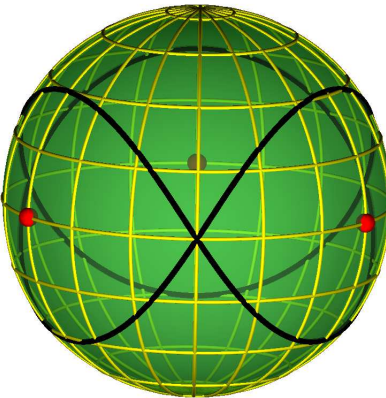


Figure 2: The shape-space sphere: the figure-eight orbit (solid black curve); three two-body collision points (bold red), singularities of the potential, lie on the equator.

the total energy scales as $E \rightarrow \alpha^{-1}E$, and the period T as $T \rightarrow \alpha^{3/2}T$. Consequently, the combination $|E|^{3/2}T$ is invariant under scale transformations and we shall call it scale invariant period $T_{\text{s.i.}} = |E|^{3/2}T$.

C. Choice of Initial Conditions

We use the property that “with the exception of Lagrange’s solution, every solution with zero angular momentum to the Newtonian three-body problem suffers syzygies” [62], [37], to allow us to always choose a collinear configuration for the initial conditions, without losing any potential periodic solutions. This second constraint further reduces the dimension of phase space by one, and leaves a four-dimensional space of initial conditions for periodic orbits.

To make the search within this nonlinear four-dimensional space more manageable, we further reduce its dimension by a judicious choice of the initial configuration. A useful tool for doing this reduction is symmetry. For three equal masses, the only remaining symmetry is three-body permutation symmetry – both the kinetic and the potential energies are symmetric under permutations. So, it is reasonable to choose an initial configuration that respects the permutation symmetry of the problem.

Perhaps the simplest way of reducing the dimension of the search space is to take an initial point on the equator and/or one of three symmetry, or Euler meridians on the shape sphere. The most symmetric initial configuration is the Euler point itself: it corresponds to

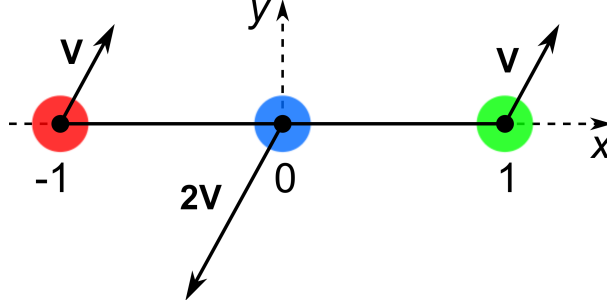


Figure 3: Geometry of the initial conditions – symmetric configuration with parallel velocities.

a collinear configuration, with one body exactly in the middle between the other two (see Fig. 3).

The rest of the initial conditions are determined by the condition that the time derivative of the hyperradius vanishes at the initial time $\dot{R}|_{t=0} = 0$ and that the angular momentum vanishes. We continue to use these two conditions, although they can and should be relaxed in the future. In this subspace of the full initial condition phase space, the three particles' initial conditions are specified by only two parameters, the initial velocities $\dot{x}_1(0)$ and $\dot{y}_1(0)$. The other initial conditions are given by $x_1(0) = -x_2(0) = 1$, $x_3(0) = 0$, $y_1(0) = y_2(0) = y_3(0) = 0$, $\dot{x}_2(0) = \dot{x}_1(0)$, $\dot{x}_3(0) = -2\dot{x}_1(0)$, $\dot{y}_2(0) = \dot{y}_1(0)$, and $\dot{y}_3(0) = -2\dot{y}_1(0)$. Therefore this two-dimensional subspace can be parametrized with components of the velocity 2-vector ($v_x = \dot{x}_1(0)$, $v_y = \dot{y}_1(0)$) (see Fig. 3). Note that only a limited region of this subspace corresponds to negative energies, that is, to bounded motions.

III. IDENTIFICATION OF PERIODIC ORBITS

If two periodic orbits of three identical particles with different values of positions and velocities can be turned one into another by means of some or all of the following transformations: translation, scaling and rotation, then they are said to be described by mathematically equivalent solutions. These are the trivial tests of identity of an orbit. One may have two different periodic orbits that have identical topologies, however.

The idea of using the topology of a three-body orbit to identify and/or classify it, was apparently conceived by Moore [16], who used the braid group B_3 to identify individual periodic orbits. His method suffers from several drawbacks: 1) it works only for absolutely

periodic orbits in two-dimensional space. This means that relatively periodic orbits cannot be classified, unless their motion is in a plane, and the rotation angle is commensurate with π ; 2) even with the above provisos, there are some orbits that cannot be classified according to this method, e.g. the Lagrange and Euler orbits; and 3) it cannot be used to classify orbits into families that differ (only) by different values of the angular momentum.

Montgomery [34] devised another method of identification and classification, based on the topology of the periodic orbit on the shape sphere – there the topology of an orbit is expressed algebraically as an element of the free group F_2 on two letters, see Sect. II B.

That method overcomes the above two shortcomings of Moore’s method, but has shortcomings of its own, [26]: there is an intrinsic ambiguity in this method that allows, at least the possibility of up to three distinct (conjugacy classes of) free group elements for each topology. This ambiguity can be resolved in the case of orbits found thus far and presented in this paper, by using the symmetries of these orbits. That resolution does not always work in general: e.g. for orbits that do not pass through any of Euler’s points.

Other sequences of symbols have been used in the literature for the purposes of identification and classification, but they all suffer from the same ambiguity problem as Montgomery’s scheme. That appears to be related to an old unsolved mathematical problem (automorphisms of free groups), [26].

We shall use Montgomery’s method here, so we give its description in Sect. III A below, together with a brief outline of its ambiguities, in Sect. III B.

A. Montgomery’s topological identification method

A periodic three-body orbit is represented by a closed curve on the shape sphere. A curve corresponding to a collisionless periodic orbit can not pass through any one of the three two-body collision points. Stretching this curve across a collision point would therefore change its topology. The classification problem of closed curves on a sphere with three punctures is given by the conjugacy classes of the fundamental group, which is in this case the free group on two letters (\mathbf{a}, \mathbf{b}), see Fig. 4.

This abstract notation has a simple geometric interpretation: it classifies closed curves in a plane with two punctures according to their topologies. The shape sphere can be mapped onto a plane by a stereographic projection using one of the punctures as the north pole,

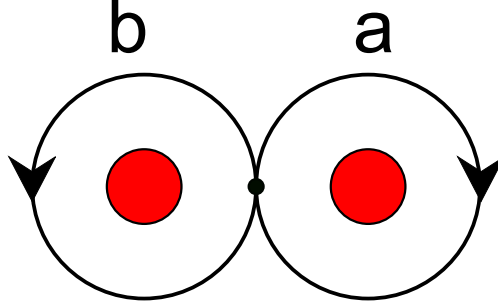


Figure 4: The two elements (a, b) of the free group.

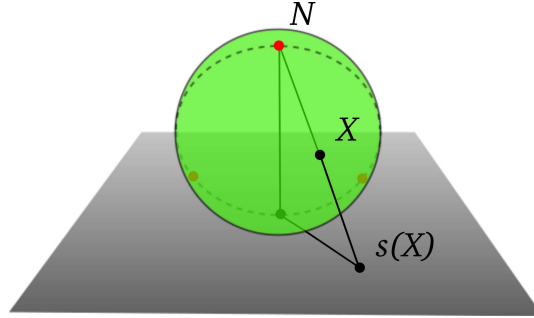


Figure 5: Stereographic projection of a sphere onto a plane. Three two-body collision points (solid red) lie on a meridian (dashed circle), with one of them being at the north pole (denoted by the letter N).

see Fig. 5. The selected puncture is thusly removed to infinity, which leaves two punctures in the (finite) plane. Any closed curve on the shape sphere (corresponding to a periodic orbit) can now be classified according to the topology of its projection in the plane with two punctures. Topology of a curve can be algebraically described by a “word” - a sequence of letters \mathbf{a} , \mathbf{b} , \mathbf{A} and \mathbf{B} - which is, more formally, an element of the free group F_2 . Here \mathbf{a} denotes a clockwise full turn around the right-hand-side puncture, \mathbf{b} the counter-clockwise full turn around the left-hand-side puncture (see Fig. 4), and the upper case letters denote their inverse elements $\mathbf{a}^{-1} = \mathbf{A}$ and $\mathbf{b}^{-1} = \mathbf{B}$.

A specific periodic orbit can be equally well described by several different sequences of letters. As there is no preferred starting point of a closed curve, any other word that can be obtained by a cyclic permutation of the letters in the original word represents the same curve.

The conjugacy class of a free group element (word) contains all cyclical permutations of the letters in the original word. For example, the conjugacy class of the free group element

\mathbf{aB} also contains the cyclically permuted word \mathbf{Ba} . The class of topologically equivalent periodic orbits therefore corresponds not merely to one specific free group element, but to the whole conjugacy class.

Time-reversed orbits are represented by the inverse elements of the original free group elements. Naturally, they correspond to physically identical solutions, but they generally form different words (free group elements) with different conjugacy classes.

Another ambiguity is related to the choice of the puncture to be used as the north pole of the stereographic projection (of the sphere onto the plane). A single loop around any one of the three punctures on the original shape sphere (denoted by \mathbf{a} or \mathbf{b}) must be equivalent to the loop around the either of the two remaining punctures. But as can be seen in Fig. 5, a simple loop around the third (“infinite”) puncture on the shape sphere corresponds to \mathbf{aB} , a loop around both poles in the plane. Therefore, \mathbf{aB} must be equivalent to \mathbf{a} and \mathbf{b} .

For example, the figure-eight orbit, [16, 17], drifts along the equator on the shape sphere and simultaneously moves between the northern and southern hemisphere, thus “slaloming” among the two-body singularities, see Fig. 2. This orbit is related to the conjugacy class of the word \mathbf{abAB} in any convention, i.e., with arbitrary choice of the north pole, [20].

Some periodic solutions have free group elements that can be written as $w^k = w^k(\mathbf{a}, \mathbf{b}, \mathbf{A}, \mathbf{B})$, where $w = w(\mathbf{a}, \mathbf{b}, \mathbf{A}, \mathbf{B})$ is a word that describes some solution, and k is an integer. Such orbits will be called topological-power satellites. For example, the orbits with free group element $(\mathbf{abAB})^k$ are called figure-eight (k) satellites, and are all free from the stereographic projection ambiguity. For further examples see Sec. IV.

B. Resolving the ambiguity in Montgomery’s method

The ambiguity mentioned above can be resolved by applying the stereographic projection of the shape sphere onto a plane with one particular puncture chosen as the north pole.

The equal mass three-body Newtonian potential has (discrete) symmetries that can be represented on the shape sphere. There are three meridians on the shape sphere that correspond to three binary permutations, or transpositions, S_2 subgroups of the full permutation group S_3 . Two rotations by $\phi = \pm 2\pi/3$ about the axis passing through the north and south poles correspond to two cyclic three-body permutations. Note the symmetry of the potential under the reflections about the three “transposition meridians” and the two rotations.

These symmetries of the potential are reflected in the symmetries of the periodic orbits that pass through one of Euler points, that is, the intersections of the symmetry meridians and the equator on the shape sphere. All of our solutions are symmetric under reflections about the (initial) Euler point, see [20]. Therefore it seems natural to use the two-body collision point opposite the “symmetry Euler point” as the north pole of the stereographic projection. That convention removes the ambiguity.

The word describing an orbit is unambiguous for orbits that are invariant under cyclic permutations of three punctures on the shape sphere. So far, there are only four known examples of such: one of them is the figure-eight orbit (and its topological-power satellites); the remaining three are the new non-figure-eight choreographies found in Ref. [24].

Changing the puncture that defines the north pole of the stereographic projection defines transformations/mappings of words that are known in mathematics as automorphisms of a free group, and form one of the oldest open problems in the theory of free groups, [26]. Effects of automorphisms on conjugacy classes, and in particular on the number of classes equivalent under such automorphisms, are not known in general. But, computations of conjugacy classes of specific words can be implemented using an electronic computer.

C. Alternative to Montgomery’s method

There is an alternative method, Ref. [35], of assigning a sequence of three symbols, in this case three digits, to any given “word” in the free group F_2 . The rules for converting “words” consisting of letters **a**, **b**, **A**, **B** into “numbers” consisting of three digits - (1, 2, 3) - are as follows: (i) make the substitution **a** = 12, **A** = 21, **b** = 32, **B** = 23; (ii) 11 = 22 = 33 = empty sequence (“cancellation in pairs rule”). So, for example:

(1) the symbolic sequence corresponding to the BHH family of orbits, **aB** = 1223 = 13 is equivalent, by way of cyclic permutations, to: **a** = 12 and to **B** = 23, as one would expect intuitively. Thus we see that the “lengths” N_n , i.e., the number of symbols/numbers in a sequence are identical for all three symbolic sequences representing the BHH family, $N_n(13)=N_n(12)=N_n(23)$, see Sect. IV B, unlike the Montgomery’s method, where $N_w(\mathbf{aB}) \neq N_w(\mathbf{a}) = N_w(\mathbf{B})$. This indicates that the “lengths” $N_n(w)$ are good algebraic descriptors of the complexity of an orbit’s topology.

(2) the symbolic sequence **abAB** = (12)(32)(21)(23) = 12322123 = 123123 = (123)²

corresponding to the figure-eight orbit is now manifestly invariant under cyclic permutations, $1 \rightarrow 2 \rightarrow 3$ and $1 \rightarrow 3 \rightarrow 2$, whereas it is so only in a non-manifest way in the two-letter scheme. Here, also, the “length” $N_n(w)$ is also a good algebraic descriptor of the complexity of an orbit’s topology.

The numbers 1, 2, and 3 can be viewed as denoting syzygies, i.e., crossings of the equator on the shape sphere, in one of three corresponding segments on the said equator. Note that (i) each symbol/number is its own inverse, which accounts for the “cancellation in pairs” rule[63] This circumstance leads to the reduction (by a factor of two) of the number of symbolic sequences denoting one topology, as the time-reversed orbit has an identical symbolic sequence to the original one (which is not the case in the two-letter scheme); and (ii) that the cyclic permutation symmetry indicates irrelevance of which syzygy is denoted by which digit.

In this way, one restores the three-body permutation symmetry of the problem into the algebraic notation describing the topology of a periodic three-body orbit, albeit at the price of having three symbols, rather than two. This restoration of permutation symmetry also implies an absence of the “automorphism ambiguity” discussed in Sect. III B. Such three-symbol sequences have been used e.g. in Ref. [35] to identify the topology of periodic three-body orbits.

The length of a sequence of symbols necessary to describe any given topology generally increases by a factor close to 1.5 as one switches from two letters N_w to three digits N_s , as symbols used, i.e., $N_s \simeq 1.5N_w$. The precise value of this proportionality factor ($\simeq 1.5$) is not important for our purposes, as we shall be concerned with the length(s) of symbolic sequences with a well-defined algebraic form, such as $\mathbf{w}_1(\mathbf{w}_2)^n\mathbf{w}_3(\mathbf{w}_4)^n$, where $n = 1, 2, 3, \dots$. In such a case, the following relation holds $N[\mathbf{w}_1(\mathbf{w}_2)^n\mathbf{w}_3(\mathbf{w}_4)^n] \simeq nN[\mathbf{w}_1(\mathbf{w}_2)\mathbf{w}_3(\mathbf{w}_4)]$ using any/either set of symbols for \mathbf{w}_i . Only the value of the slope parameter changes as one switches from one set to another. Of course, it is an additional mystery if and when the slopes of different sequences happen to coincide.

IV. BRIEF OVERVIEW OF EARLIER RESULTS

A. Earlier periodic orbits

The numerical search and discovery of periodic three-body orbits can be roughly divided into five periods.

1. The oldest and the only solutions known in closed analytic form are those due to Lagrange and Euler, [1, 2]. They correspond to single points on the shape sphere – the north (or south) pole for the Lagrange solution, and the Euler point for the Euler solution. Such a “curve” on the shape sphere has a trivial topology, corresponding to the word $w = \mathbf{a}^0 = \mathbf{e}$, i.e., the unit free group element. The hyper-angular degree of freedom on the shape sphere is “frozen” in these two orbits and the dynamics is reduced to pure hyper-radial and rotational motions. There are other examples of orbits in this family, discovered numerically by Davoust and Broucke, [14], and then again by Moore, [16].
2. The second oldest family of solutions is due to Broucke-Hadjidemetriou-Hénon, [6–12]. It has trajectories in the form of symmetrical ovals on the shape sphere, with word $w = \mathbf{aB}$ describing its topology (in our ambiguity-fixing convention, Sect. IIIB). These ovals have two axes of symmetry: the Euler or symmetry meridian, and the equator, and are centered on one of the two-body collision points. This symmetry was used in the process of their numerical construction in Refs. [6–9]. Topological-power satellites with topologies $w = (\mathbf{aB})^k$, with $k \leq 3$ of a few BHH orbits $w = \mathbf{aB}$ were first reported by Davoust and Broucke, [14]. Many such satellites, with $k \leq 58$, have been found using a different method in Ref. [27], many of which solutions do not have the symmetry conjectured and used in Refs. [6–9].
3. The third oldest family contains isosceles triangle orbits (related to the post-Moore-an “dragonfly” orbit from Ref. [20]), with topologies described by the free group element $w = \mathbf{b}^2\mathbf{A}^2$, discovered by Davoust and Broucke, and studied further in Ref. [14], (denoted as family A2 in Strömgren’s notation).
4. The fourth oldest family contains Moore’s and Simó’s figure-eight solutions, as well as their satellites, Refs.[16–18, 21]. These solutions have a truly global form on the shape

sphere, encircling it twice (see Fig. 2). The figure-eight orbit’s topology is described by the word **abAB**. Šuvakov [21] and Šuvakov and Shibayama [24] searched and found more than 20 distinct topological power satellites of the figure-8 orbit.

5. More than a dozen of recent post-Moore-an solutions, Refs. [20, 22, 23, 38].

B. Period vs. topology relation

As a consequence of those discoveries and of the application of Montgomery’s method, one could, for the first time, look for relations between the topological and dynamical properties of orbits. At first, in Ref. [21], an approximately linear functional relation was noticed:

$$\frac{T_{\text{s.i.}}(w^k)}{T_{\text{s.i.}}(w)} \equiv \frac{T(w^k)|E(w^k)|^{3/2}}{T(w)|E(w)|^{3/2}} \simeq k = 1, 2, 3, \dots, \quad (5)$$

where T is the period, E the energy and $w = \mathbf{abAB}$ the free-group element of the figure-eight orbit, and $w^k = [\mathbf{abAB}]^k$, ($k = 1, 2, 3, \dots$) are the free-group elements of its k -th “topological-power satellite” orbits, see Sect. III A, all with zero angular momentum. The \simeq sign here means equality within the estimated numerical precision.

In the meantime several examples have been found with improved numerics where this relation breaks down at higher decimal places.

Initially, only the “topological-power satellites” of the figure-eight orbit were known, [21, 24], with one exception: the yarn orbit $w_{\text{yarn}} = (\mathbf{babABabaBA})^3 = w_{\text{moth I}}^3$ in Ref. [20], where $w_{\text{moth I}} = \mathbf{babABabaBA}$.

In the meantime we have found four new examples of topological-power satellites of the “moth I” orbit, as well as several topological-power satellites of three other orbits, see Appendix A, and Ref. [25], that obey Eq. (5) within their respective numerical errors. This naturally raises the question: why do only some orbits, such as the figure-eight and the yarn one, have topological-power satellites and not others?

Following the above observation, Ref. [26] investigated all 45 orbits known at the time and not just the topological-power satellites, and proposed the following more general [64] quasi-linear relation for three-body orbits with zero angular momentum,

$$\frac{T_{\text{s.i.}}(w)}{T_{\text{s.i.}}(w_p)} \simeq \frac{N_w}{N_{w_p}} = \frac{n_w + \bar{n}_w}{n_{w_p} + \bar{n}_{w_p}}. \quad (6)$$

Here $N_w = n_w + \bar{n}_w$ is one half of the minimal [65] total number of letters, in the free group element $w = w(O)$ characterizing the family of orbit O , and similarly for $w_p = w(\text{progenitor})$, the word describing the progenitor orbit in a sequence, where n_w is the (minimal) number $n_w = \frac{1}{2}(n_a + n_b)$, of small letters **a**, or **b**, and $\bar{n}_w = \frac{1}{2}(n_A + n_B)$ is the minimal number of capital letters **A**, or **B**.

Eq. (6) appeared to define “at least four and at most six” distinct sequences among the 45 orbits in Ref. [26]. Precise algebraic definitions of these sequences, analogous to the definition w^k of the topological-power satellites, were not known at the time, again due to the dearth of distinct orbits. Many distinct satellite orbits’ points almost overlapped on the $T_{\text{s.i.}} - N_w$ graph, due to identical values of N_w and similar periods, which further reduced the number of distinct data points. Moreover, there were significant “gaps” between the data points, as well as one “outlier point” (orbit), that was roughly 8% off the conjectured straight line. All of this left one with a (general) feeling of incompleteness.

Equation (6) predicts infinitely many new, as yet unobserved orbits together with their periods; if true, even approximately, Eq. (6) would be a spectacular new and unexpected property of three-body orbits, that would open new inroads into understanding the Newtonian three-body problem, as well as help in practical searches to find new orbits. Therefore Eq. (6) merits a thorough investigation.

V. OVERVIEW OF OUR RESULTS

Before plunging into the details, we wish to give an overview of our results.

Following the lead presented in Ref. [26], we used Eq. (6) first to predict the periods and numbers of letters of new orbits, and then to search for them. We searched by first identifying the linearly stable orbits among the original 13 orbits, and then by “zooming in” our search on smaller windows around the stable orbits: Thus we found new periodic orbits that have “filled” many of the “gaps” in the $T_{\text{s.i.}} - N_w$ graph, see Fig. 6, the Appendix A, the web site [25] and Ref. [38]. The “outlier” point has become just another orbit in a new sequence with a slightly steeper slope on the same graph. Thus, it has become clear that the periods do not lie on one straight line, but rather on several lines with slightly different slopes, emerging from a small “vertex” area, forming a (thin) wedge-like structure.

All newly found orbits, Appendix A, fit into ten sequences, where the fourth (“moth I”)

sequence from Ref. [26] has been divided into three: a) “moth I $(n, n + 1)$ ”; b) “butterfly III-IV $(n, n + 1)$ ”; c) “moth III $(n, n + 1)$ ”. Moreover, we found two entirely new sequences: 1) “VIIa moth (n, n) ” and 2) “VIIb moth (n, n) ”, and one sequence of pure “topological-power satellites” of the moth I orbit. Each of these ten sequences has associated with it an algebraic pattern either in terms of free-group elements, Table I, or in terms of three-digit “numbers”, Table II.

Here we shall use the sequence label (n, m) to denote the general form of (n_w, \bar{n}_w) in that sequence: for example (n, n) means that n_w and \bar{n}_w are equal integers: $n = n_w = \bar{n}_w = 1, 2, 3, \dots$. Then, n can be used to label orbits within the sequence, Appendix A. By setting $n = 0$, or $n = 1$, as may be the case depending on the sequence, in the second column of Table I we can read off the topologies of the respective progenitors of each sequence and thus identify the progenitor, see Table V.

The individual $T_{s.i.} - N_w$ graphs, with a description of topologies in terms of free-group elements are shown in Figs. 7, 8, their free-group patterns are shown in Table I. The agreement of separate sequences with the linear functional Ansatz, Eq. (6), see Figs. 7, 8, is much better than for the aggregate of all orbits, Fig. 6(a), but the (root-mean-square) variations of line parameters (a, b) reported in Table I are generally larger than the estimates numerical errors, *thus indicating that Eq. (6) is approximate, and not exact in these sequences.*

The corresponding $T_{s.i.} - N_w$ graphs, with a description of topologies in terms of three syzygies (equator-crossings) denoted by numbers (1,2,3) are shown in Figs. 9, 10, their free-group patterns are shown in Table II. The agreement of separate sequences with the linear functional Ansatz, Eq. (6), see Figs. 9, 10, is much better than for the aggregate of all orbits, Fig. 6(b), but the (root-mean-square) variations of line parameters (a, b) reported in Table II are generally larger than the estimates numerical errors, *thus indicating that Eq. (6) is approximate, and not exact in these sequences.*

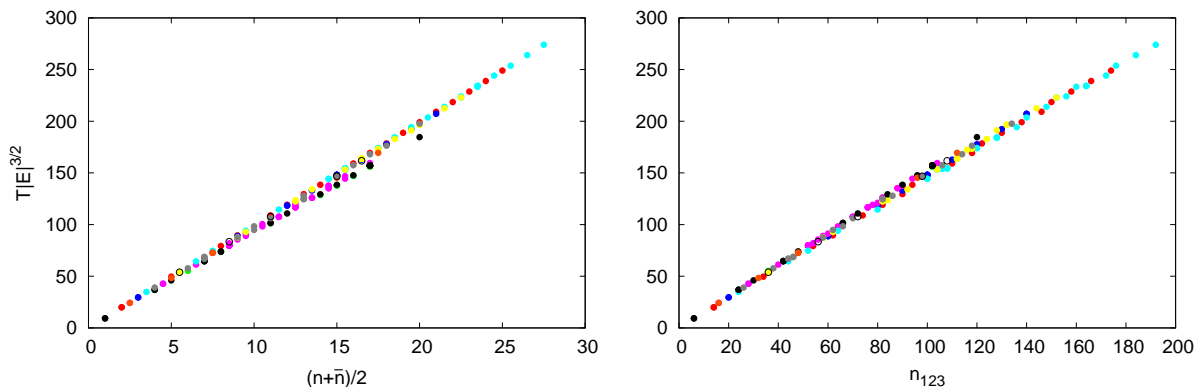


Figure 6: (color on-line) (a) Left: The scale-invariant periods $|E|^{3/2}T(w)$ of approximately 200 presently known zero-angular-momentum three-body orbits versus N_w , one half of the number of all letters in the free-group word w describing the orbit, $N_w = n_w + \bar{n}_w$, where n_w is the number of small letters a , or b , and \bar{n}_w is the number of capital letters A , or B in the letter w . (b) Right: Same as (a), only in terms of n_{123} , the number of digits in the “word” w . Color code: 1) red = sequence I - butterfly I; 2) green = sequence II - dragonfly; 3) dark blue = sequence III - yin-yang; 4) pink = sequence IVa - moth I; 5) light blue = sequence IVb - butterfly III; 6) yellow = sequence IVc - moth III; 7) black = sequence V - figure-eight; 8) orange = sequence VI - yarn; 9) grey = sequence VII - moth; 10) empty circles = other.

All orbits follow Eq. (6) fairly closely, but not exactly, as can be seen from the small, but non-negligible root-mean-square deviations (“errors”), of the line parameters a, b , in Table I. Whereas the approximate empirical rule Eq. (6) now appears established, and its extension to ever-longer periods just a technical difficulty, some deeper questions remain open. For example, the *raison d’être* of so many periodic orbits remains obscure, not to mention the underlying reason for the existence of any, let alone linear, relation among their periods.

Perhaps the first hint at a solution to the puzzle of why there should be any periodic orbits such as the topological-power satellites, was given in Ref. [27], where it was noticed that the satellite orbits, in the BHH family of orbits with non-zero angular momentum, exist only when their progenitor is linearly stable. There is a theorem, due to Birkhoff and Lewis (BL), Ref. [28], see also §3.3 (by Jürgen Moser) in Ref. [39], which holds for systems with

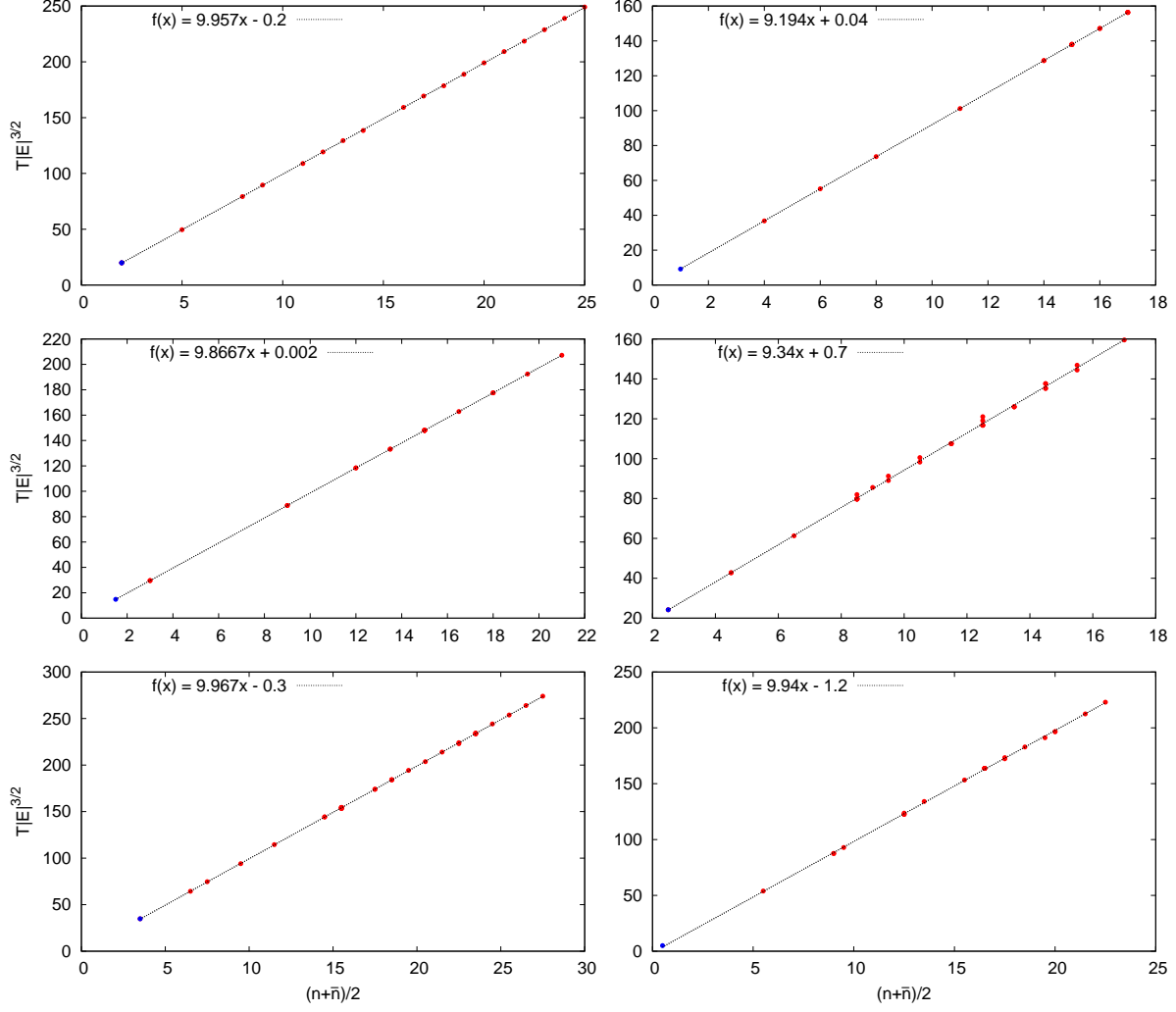


Figure 7: (color on-line) The scale-invariant periods $|E|^{3/2}T(w)$ of zero-angular-momentum three-body orbits versus N_w , one half of the number of all letters in the free-group word w describing the orbit, $N_w = n_w + \bar{n}_w$, where n_w is the number of small letters a , or b , and \bar{n}_w is the number of capital letters A , or B in the letter w . (a) Top left: sequence I - butterfly I, ; (b) Top right: sequence II - dragonfly; (c) Center left: sequence III - yin-yang; (d) Center right: sequence IVa - moth I; (e) Bottom left: sequence IVb - butterfly III; (f) Bottom right: sequence IVc - moth III. The blue points at the lower ends of sequences are the progenitors of the respective sequences, see the main text and Table I. Progenitors of sequences II, III and IVc, that involve collisions were not used in the fitting procedure, so the validity of the linear Ansatz for these sequences can be evaluated by inspection.

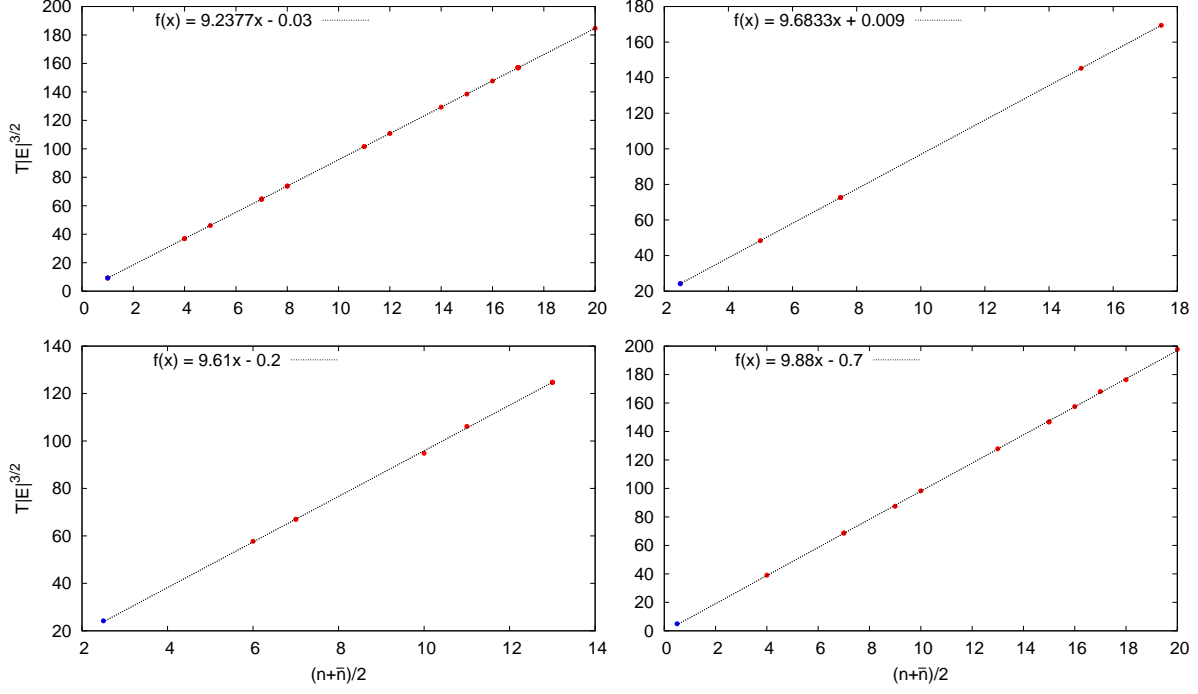


Figure 8: (color on-line) Same as in Fig. 7, except for the following sequences. (a) Top left: sequence V - figure-eight; (b) Top right: sequence VI - yarn; (c) Bottom left: sequence VIIa - moth III (n, n); (d) Bottom right: sequence VIIb - moth III (n, n). The blue points at the lower ends of sequences are the progenitors of the respective sequences, see the main text and Appendix A. The progenitors of sequence VIIa and VIIb were not used in the fitting procedure, so the validity of the linear Ansatz for these sequences can be checked by inspection.

three d.o.f. and has as a consequence, existence of infinitely many periodic orbits. [66] The Birkhoff-Lewis theorem does not say anything about the topologies, or periods of these new periodic orbits, however.

Here we conjecture that the Birkhoff-Lewis theorem may hold for periodic three-body orbits, which implies that there may be several (possibly infinitely many) linearly stable periodic orbit(s) that generate infinite set(s) of periodic orbits, with unspecified topologies and periods. We shall test this conjecture by testing one of the fundamental assumptions of the Birkhoff-Lewis theorem: the linear stability of a periodic orbit.

Given the initial conditions, linear stability of a periodic orbit can be tested numerically, see Sect. VI, and thus the applicability of the Birkhoff-Lewis (BL) theorem can be falsified.

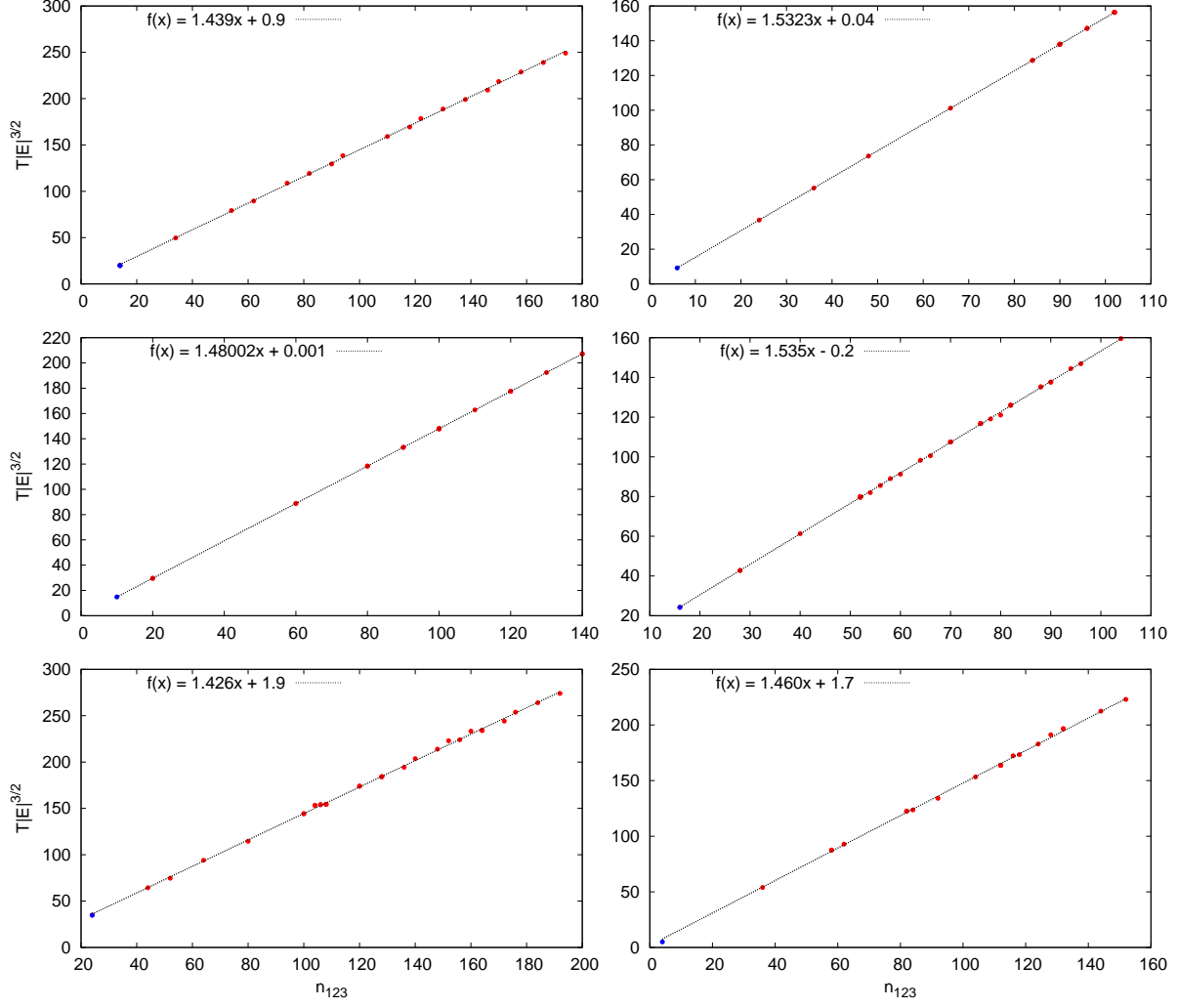


Figure 9: (color on-line) The scale-invariant periods $|E|^{3/2}T(w)$ of zero-angular-momentum three-body orbits versus n_{123} , the number of digits in the “word” w . (a) Top left: sequence I - butterfly I ; (b) Top right: sequence II - dragonfly; (c) Center left: sequence III - yin-yang; (d) Center right: sequence IVa - moth I; (e) Bottom left: sequence IVb - butterfly III; (f) Bottom right: sequence IVc - moth III. The blue points at the lower ends of sequences are the progenitors of the respective sequences, see the main text and Table I. Progenitors of sequences II, III and IVc, that involve collisions were not used in the fitting procedure, so the validity of the linear Ansatz for these sequences can be evaluated by inspection.

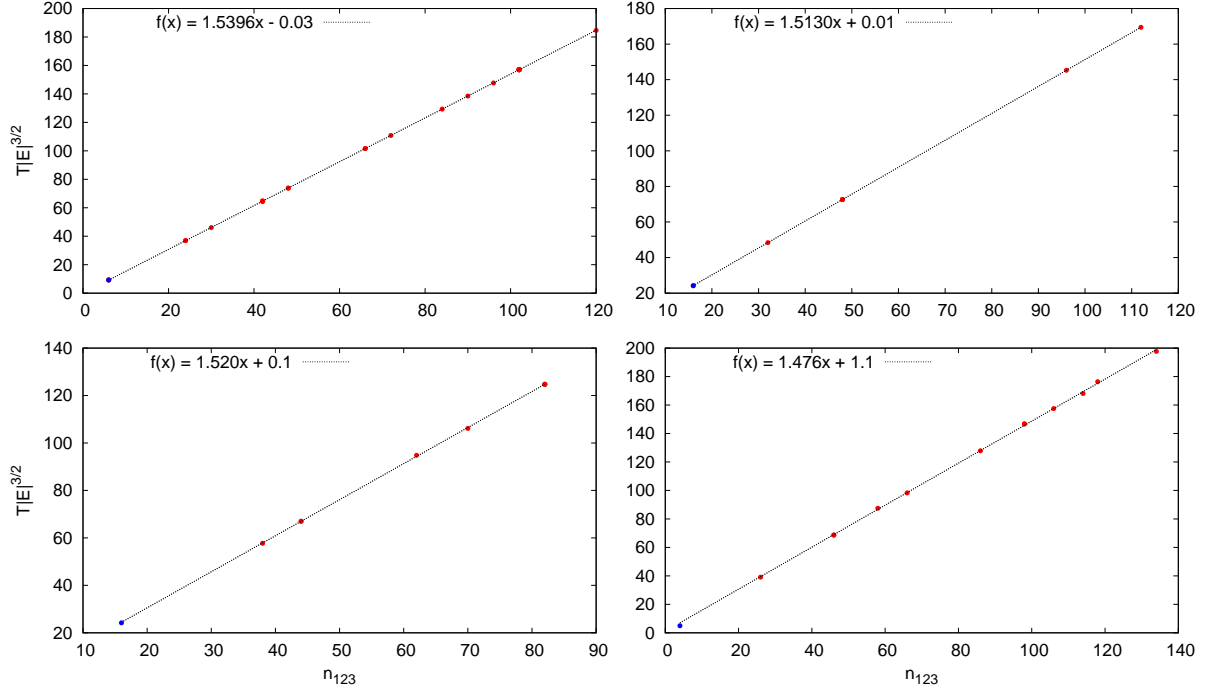


Figure 10: (color on-line) Same as in Fig. 9, except for the following sequences. (a) Top left: sequence V - figure-eight; (b) Top right: sequence VI - yarn; (c) Bottom left: sequence VIIa - moth III (n, n); (d) Bottom right: sequence VIIb - moth III (n, n). The blue points at the lower ends of sequences are the progenitors of the respective sequences, see the main text and Appendix A. The progenitors of sequence VIIa and VIIb were not used in the fitting procedure, so the validity of the linear Ansatz for these sequences can be checked by inspection.

The converse, i.e., the confirmation of the BL theorem, cannot be accomplished in this way, however, as the theorem involves other assumptions. So, until such time when all of the assumptions underlying the BL theorem have been tested, we can only discuss the conjecture of the BL theorem.

Once we establish which ones of our orbits are linearly stable, we shall show a definite correlation between the sequences in Table I and the (linear) stability of the progenitor orbit in each sequence.

Table I: Typical (non-minimal) free group elements' w structure for orbits in various sequences, the line parameters a, b , where the $T_{\text{s.i.}} - N_w$ dependence is fitted as $f(x) = ax + b$. Some orbits in a particular sequence described by the structure $w(n_i)$ may be described by words that are products of two words $w(n_i)$ with different values of index n_i .

Sequence number & name	Free group element $w(n)$	a	b
I butterfly I (n, n)	$(AB)^2(abaBAB)^n(ab)^2(ABAbab)^n$	9.957 ± 0.011	-0.2 ± 0.2
II dragonfly (n, n)	$bA(baBA)^n aB(abAB)^n$	9.194 ± 0.004	0.04 ± 0.06
III yin-yang (n, n)	$(abaBAB)^n a(babABA)^n A$	9.8667 ± 0.0003	0.002 ± 0.004
IVa moth I $(n, n+1)$	$(abAB)^n A(baBA)^n B$	9.34 ± 0.06	0.7 ± 0.7
IVb butterfly III $(n, n+1)$	$[(ab)^2(AB)^2]^n b[(ba)^2(BA)^2]^n a$	9.967 ± 0.012	-0.3 ± 0.3
IVc moth III $(n, n+1)$	$(babABA)^n A(abaBAB)^n B$	9.94 ± 0.04	-1.2 ± 0.7
V figure-eight (n, n)	$(abAB)^n$	9.2377 ± 0.0014	-0.03 ± 0.02
VI moth I - yarn $(2n, 3n)$	$[(abAB)A(baBA)B]^n$	9.683 ± 0.002	0.01 ± 0.02
VIIa moth (n, n)	$(abAB)^{(n+1)} a(baBA)^n b$	9.61 ± 0.07	-0.2 ± 0.7
VIIb moth (n, n)	$(abaBAB)^{(n+1)} b(babABA)^n A$	9.88 ± 0.04	-0.7 ± 0.5

VI. LINEAR STABILITY OF PERIODIC ORBITS

A. Definition of stability indices

The linear stability of a periodic orbit can be calculated by making use of the symplectic structure of the equations of motion; here we follow the presentation from Ref. [40].

The planar three-body system is described by means of the phase-space eight-vector

$$\mathbf{X}(t) = (\boldsymbol{\rho}(t), \boldsymbol{\lambda}(t), \dot{\boldsymbol{\rho}}(t), \dot{\boldsymbol{\lambda}}(t)).$$

in the eight-dimensional phase space. With the help of the symplectic unit matrix

$$\mathbf{J} = \begin{pmatrix} \mathbf{0} & \mathbf{1} \\ -\mathbf{1} & \mathbf{0} \end{pmatrix} \quad (7)$$

which is composed of 4×4 matrices $\mathbf{0}$ and $\mathbf{1}$, Hamilton's equations of motion can be brought

Table II: Typical (non-minimal) structure of alternative symbolic representations (“numbers”) w of periodic orbits in various sequences, in terms of three symbols (“digits”) (1,2,3). Some orbits in a particular sequence described by the structure $w(n_i)$ may be described by words that are products of two numbers $w(n_i)$ with different values of index n_i .

Sequence number & name	symbolic representation $w(n)$	a	b
I butterfly I	$\{(123)^2 2 [(123)^2 3 (321)^2 1]^n\}^2$	1.439 ± 0.007	0.9 ± 0.8
II dragonfly	$(132)^{2n} (312)^{2n}$	1.5323 ± 0.0007	0.04 ± 0.06
III yin-yang	$[(123)^2 2132]^n 231 [(123)^2 2132]^n 132$	1.48002 ± 0.00004	0.001 ± 0.004
IVa moth I	$(123)^{2n+1} 3 (321)^{2n+1} 1$	1.535 ± 0.004	-0.2 ± 0.3
IVb butterfly III	$[(123)^2 2]^{2n} 23 [(321)^2 2]^{2n} 21$	1.426 ± 0.008	1.9 ± 1.0
IVc moth III	$[(123)^2 2132]^n 23 [(321)^2 2312]^n 21$	1.460 ± 0.011	1.7 ± 1.1
V figure-eight	$(123)^{2n}$	1.5396 ± 0.0003	-0.03 ± 0.02
VI moth I - yarn	$[(123)^3 3 (321)^3 1]^n$	1.5130 ± 0.0003	0.01 ± 0.02
VIIa moth	$(123)^{2n+3} 3 (321)^{2n+1} 1$	1.520 ± 0.006	0.1 ± 0.4
VIIb moth	$[(123)^2 2132]^n 23 [(321)^2 2312]^n (321)^3 1$	1.476 ± 0.008	1.1 ± 0.7

into the compact form

$$\frac{d\mathbf{X}(t)}{dt} = \mathbf{J} \left(\frac{\partial H}{\partial \mathbf{X}} \right). \quad (8)$$

We study the behavior of solutions in the vicinity of a periodic orbit $\mathbf{X}_{\text{PO}}(t)$. After one period a trajectory with initial condition $\mathbf{X}(0) = \mathbf{X}_{\text{PO}} + \delta\mathbf{X}(0)$ reaches the point $\mathbf{X}(T) = \mathbf{X}_{\text{PO}} + \delta\mathbf{X}(T)$ in phase space, where $\mathbf{X}_{\text{PO}} = \mathbf{X}_{\text{PO}}(0) = \mathbf{X}_{\text{PO}}(T)$. One obtains the linear relation

$$\delta\mathbf{X}(T) = \mathbf{M}(\mathbf{X}_{\text{PO}}; T) \delta\mathbf{X}(0) \quad (9)$$

between an infinitesimal initial deviation $\delta\mathbf{X}(0)$ and the final deviation $\delta\mathbf{X}(T)$. In Eq. (9) \mathbf{M} is the so-called monodromy matrix with elements defined as

$$\mathbf{M}_{ij}[\mathbf{X}_{\text{PO}}; t] := \frac{\partial \mathbf{X}_i(t)}{\partial \mathbf{X}_j(0)} \quad (10)$$

and represents the linear approximation to the phase-space flux around the periodic orbits. From Eqs. (8) and (10) one obtains the equations of motion for \mathbf{M} ,

$$\frac{d\mathbf{M}}{dt} = \mathbf{J} \left(\frac{\partial^2 H}{\partial \mathbf{X}^2} \right) \mathbf{M}, \quad \mathbf{M}(0) \equiv \mathbf{1}$$

which allows one to integrate \mathbf{M} along a periodic orbit.

The stability of a periodic orbits is determined by means of eigenvalues λ of $\mathbf{M}(T)$, which come in pairs, or quadruplets: if λ is an eigenvalue of \mathbf{M} so are $1/\lambda$, λ^* , and $1/\lambda^*$. They are classified as follows. (i) *elliptical*, if $\lambda = \exp(\pm 2\pi i\nu)$ with the (real) stability angle ν describing the stable revolution of adjacent trajectories around a periodic orbit. (ii) *(inverse) marginally stable* if $\lambda = +1$ ($\lambda = -1$). (iii) *(inverse) hyperbolic* if $\lambda = \exp(\pm\mu)$ [$\lambda = -\exp(\pm\mu)$] where $\mu > 0$ (real) is the stability exponent of the periodic orbit, sometimes called the Lyapunov exponent of the periodic orbit. (iv) *Loxodromic* if $\lambda = \exp(\pm\mu \pm i2\pi\nu)$, with μ, ν being real numbers. The loxodromic case is peculiar to systems with more than two degrees of freedom, such as the three-body problem. We calculate the “winding numbers” ν and the Lyapunov exponents μ by numerical integration of \mathbf{M} , Sect. VIB.

B. Calculation of stability indices

We have analyzed linear stability of all (around 200) zero-angular-momentum non-colliding orbits from the present paper and Refs. [20, 21, 24]. We have used a symplectic code with quadruple precision, regularization of collisions, and a monodromy improvement. The values displayed in Tables III and IV are the results of this code.

About 20 orbits are linearly stable, as shown in Table III. They are “moth I”, “moth II”, and “bumblebee” from Ref. [20], and the figure-eight orbit, Refs. [18, 19], its seventh topological-power - choreographic satellite, as well as two 17th topological-power non-choreographic satellites, Ref. [24]. Two of these orbits’ (figure-eight orbit, and its seventh topological-power) stability had been studied earlier, whereas the stability of orbits V.17.H = O13, V.17.I = O14 and V.17.J = O15 is new, where notation O# is from Ref. [21]. From the equality of the stability coefficients for the orbits V.17.I = O14 and V.17.J = O15, we conclude that these two sets of initial conditions describe one and the same orbit. Orlov’s (colliding) S-orbit’s stability had not been studied before, to our knowledge.

In Table IV we show several marginally stable orbits that have very small values of the

Lyapunov exponent μ , that is numerically almost consistent with being zero.

All of these orbits deserve further study, with regard to extensions to non-zero angular momentum and to unequal mass ratios, as they might be of astronomical interest (see Sect. VIII).

Table III: The stability angles ν_j , where $\lambda_j = \exp(\pm 2\pi i \nu_j)$ define the linear stability coefficients of linearly stable periodic three-body orbits.

Label	ν_1	ν_2
S-orbit	0.131093	0.470591
Moore 8	0.298093	0.00842275
NC1 (8^7)	0.27216	0.158544
V.17.H (O13 = 8^{17})	0.31573	0.0002988
V.17.I (O14 = 8^{17})	0.0435411	0.00262681
V.17.J (O15 = 8^{17})	0.0435411	0.00262681
II.11.A (bumblebee)	0.137149	0.0325135
IVa.2.A (moth I)	0.159013	0.491881
IVa.4.A (moth II)	0.108451	0.0886311
I.5.A	0.170764	0.001476
I.14.A	0.443006	0.000121435
II.17.B	0.138698	0.0335924
III.13.A. β	0.175816	0.000655417
IVb.3.A (butterfly III)	0.378728	0.00173642
IVb.9.A	0.194186	0.000561819
IVc.12.B	0.0863933	0.00394124
IVc.17.A	0.0442047	0.00206416
VIIa.11.A	0.416228	0.0088735
VIIb.7.A	0.27753	0.0360425
VIIb.9.A	0.216455	0.0584561
VIIb.13.A	0.0621421	0.0141894

Table IV: Marginal orbits’ stability angle ν , defined by the elliptic linear stability coefficient λ_i as $\lambda = \exp(\pm 2\pi i\nu)$, and the Lyapunov exponent μ , defined by $\lambda = \exp(\pm\mu)$, of stable-marginal orbits, or possibly hyperbolic (unstable) orbits. We display orbits with $\mu \leq 0.05$, which we fix as the upper limit on the numerical error.

Label	ν_1	μ_2
I.2.B (butterfly II)	0.0582152	0.0169623
III.12.A. α	0.255754	0.00301844
IVb.6.A	0.2182410	0.0150196
IVc.21.A	0.185333	0.0022804
VIIb.17.A	0.462192	0.0028639

VII. LINEAR STABILITY OF PROGENITOR ORBITS

Two linearly stable orbits (“butterfly III”, “moth I”) lie at the origins of two “linear sequences” of “non-topological-power satellite” orbits observed among the original 13 orbits from Ref. [26].

Thus, the manifest candidates for collisionless progenitors are: 1) “figure-eight” for the sequence V “figure-eight (n, n) ”; 2) “moth I” for the sequence IVa “moth I $(n, n + 1)$ ”, as well as for the sequence VI “moth I - yarn $(2n, 3n)$ ”; and 3) “butterfly III” for the sequence IVb “butterfly III $(n, n + 1)$ ”.

These three progenitors are collisionless orbits with three degrees-of-freedom, that are linearly stable. The existence of many periodic orbits in their sequences, suggest that these three progenitors might satisfy the conditions of the Birkhoff-Lewis theorem. We note here that another, collisional orbit might be taken as the progenitor of sequence IVb “butterfly III $(n, n + 1)$ ”, albeit with a smaller value of the index n : the Schubart orbit, Ref. [5].

Next we extend the kind of reasoning found in Ref. [24] to sequences of periodic three-body orbits with collisional progenitors.

1) The Schubart orbit, Ref. [5] is the progenitor of four (five) sequences: I, IVb, (IVc), VIIa and VIIb, see Table I and Appendix A. The Schubart orbit is linearly stable in three spatial dimensions, [6, 7], but due to its collinear nature, it has only two degrees-of-freedom.

As it has two degrees-of-freedom, it satisfies the Poincaré-Birkhoff theorem, [41–43], which predicts the existence of infinitely many orbits. Thus, one collisional orbit is the progenitor of more than one sequence of collisionless orbits.

2) The parent orbit of sequence II “dragonfly (n, n) ” is Broucke’s isosceles triangle orbit, Refs. [13, 14], that involves (two-body) collisions. This orbit always stays in an isosceles triangle configuration, thus eliminating one hyper-angle from being a dynamical degree-of-freedom, and is linearly stable, Refs. [13, 44], so it also satisfies the Poincaré-Birkhoff theorem.

3) The parent orbit of the “yin - yang” sequence is the collisional “S-orbit” of Refs. [22, 23] (see the initial condition # 20 in Table I, Ref. [23]) that is linearly stable.

Table V: The progenitor orbits of various sequences, and their stability. The check mark indicates that the orbit is linearly stable.

Sequence number & name	progenitor	stability
I butterfly I (n, n)	Schubart	✓
II dragonfly (n, n)	isosceles	✓
III yin-yang (n, n)	S-orbit	✓
IVa moth I $(n, n + 1)$	moth I	✓
IVb butterfly III $(n, n + 1)$	butterfly III	✓
IVc moth III $(n, n + 1)$	Schubart	✓
V figure-eight (n, n)	figure-8	✓
VI moth I - yarn $(2n, 3n)$	moth I	✓
VIIa moth (n, n)	Schubart	✓
VIIb moth (n, n)	Schubart	✓

Provided the above progenitor orbits satisfy the remaining (“twist”) condition of the Birkhoff-Lewis theorem, there is a simple and natural explanation of the existence of infinitely many topological-power satellites, as well as of orbits with the same number of letters. We emphasize, however, that the Birkhoff-Lewis theorem makes no mention of topology or its connection with the periods of orbits.

We note here that in 1976 Hénon, Ref. [6], established the linear stability of many orbits in

the BHH family, that have non-vanishing angular momenta ($L \neq 0$). The topological-power satellites of the linearly stable BHH orbits were discovered only recently, Ref. [27], where an $L \neq 0$ version of the period-topology linear dependence Eq. (6) was checked numerically, as well. The agreement is only approximate, however, as a small, but numerically significant discrepancy exists [67]. This appears as another manifestation of the Birkhoff-Lewis theorem.

We have also shown that some of the longer-period (“satellite”) orbits are linearly stable, for example the seventh satellite of “figure-8” orbit, established in Ref. [24, 29]; the moth II, which lies in the “moth I” sequence; the “bumblebee” orbit, which is in the “dragonfly” sequence; as well as others. These orbits may generate infinite sequences of their own.

VIII. SUMMARY, CONCLUSIONS AND OUTLOOK

In summary, we have:

- 1) found more than 150 new periodic orbits and determined their topologies. We classified these 150 plus all previously known orbits in 10 sequences with periods that grow approximately linearly with the number of “letters” describing the orbit’s topology.
- 2) tested their stability: six are linearly stable in three independent calculations; 12 in two independent calculations, and six are (close to being) marginal in two independent calculations.
- 3) shown that the shortest-period orbit in each sequence is linearly stable, which is in agreement with the Birkhoff-Lewis and Poincaré-Birkhoff theorems, which posit that there are infinitely many orbits around linearly stable orbits with three and two degrees of freedom, respectively.

We hope to have convinced the reader that there are infinitely many new periodic orbits still to be discovered within the present subspace of the full phase space, as well as regularities among these orbits that remain to be explored, let alone fully understood. Of course, the discovery of such new orbits with ever-longer scale-invariant periods, hinges on improvement of the numerical methods used. Moreover, there are other orbits to be searched for outside the present search subspace. During the final preparation of this manuscript we have discovered the recent numerical searches by Rose [59] and by Li and Liao [60].

Here we wish to express our expectation that at least some of these (topological types of) orbits will be discovered in direct astronomical observations, see the discussion below.

Moreover, our present results naturally raise several astronomical, astrophysical, as well as mathematical questions.

Astronomy

It is well known that certain subsystems within the Solar System can be viewed as (almost) periodic solutions of the general three-body problem, see e.g. Sect. 14. in Ref. [8]. All of those orbits are hierarchical and thus belong to the BHH family. That does not include the Jovian, as well as other trojans, which are Lagrangian solutions. Altogether more than 3000 exoplanets have been confirmed by various detection methods, including the Kepler mission. Among them there are at least 597 multiple planetary systems that contain three-body (sub)systems [45].

Therefore, it would seem worthwhile to examine this data set for topologically distinct three-body systems [45]. As it is not easy to nail down the orbital parameters from the observed data, the topology of the orbit should be used as a clear/unambiguous benchmark – after all, it is the topology, rather than the kinematical properties, that distinguishes one family of orbits from another.

The first question is: are all such three-body subsystems hierarchical? If not, then what are their topologies? One does not need to know dynamical details, such as masses, velocities, orbital parameters, in order to determine the topology of a three-body orbit, only the ordering of syzygies, which might be feasible with the present data.

For such a question to be answered, however, one needs a comprehensive compilation of presently known three-body orbits’ data, to compare with. Although reviews of three-body systems are published on a more-or-less regular basis, they generally do not contain systematic compilations of new periodic orbits’ data, see e.g. [45]. For this reason, we have formed the web site [25] that contains the initial conditions, as well as other pertinent data regarding periodic three-body orbits known to us at the present time. We hope that our results will encourage and facilitate such a search for exotic three-body systems within the Kepler data.

Astrophysics

Every periodic orbit with zero angular momentum and equal masses defines the starting point of an infinite family of orbits with the same topology and equal masses, but different angular momenta that change continuously from one to the next. Similarly, every periodic orbit with equal masses defines a starting point of an infinite set of orbits with the same

topology and angular momentum, but different mass ratios. As the mass ratios and/or angular momenta change, so do the stability coefficients. Nevertheless, as a consequence of continuity, one may reasonably expect to find some, perhaps small, region of stability around each stable orbit with zero angular momentum and equal masses. Therefore, every new, linearly stable periodic orbit deserves to be thoroughly examined with regard to changes of the angular momentum and/or mass ratios, just as it was done in the case of the BHH family in Refs. [6–12]. That is, of course, a lot of hard work yet to be done, but the probability of finding equal mass three-body systems with zero angular momentum in astronomical observations is negligible. But, even if a particular family of orbits remains stable in substantial region(s) of the (mass-ratio, angular momentum) parameter space, there is no guarantee that orbits of that sort actually exist in the Universe, much less that they will be observed within a finite time. Thereafter, specific formation scenarios will have to be checked, which is a task for theoretical astrophysicists.

Another, different, task is to explore post-Newtonian corrections to the Newtonian solutions: all of the (multiple) exoplanetary systems observed thus far are non-relativistic. This need not be the case in triple star systems, in particular in triple systems containing one or more compact stellar objects (neutron stars and/or black holes). More than 900 triple star systems have been observed: the vast majority of which are hierarchical, Ref. [46]. The number of confirmed triple star systems containing one or more compact stellar objects is one, [47], at the moment, to our knowledge.

Relativity must play a role in the double-compact star/black hole triple star systems, so our study must be extended to include relativistic effects, including gravitational radiation. The latter had been studied in a few special cases of non-relativistic periodic three-body motion, see Refs. [48–51], before the recent observations of gravitational waves were reported, [53, 54]. Whereas it was widely expected that binary collisions of two black holes are the primary sources of gravitational waves observed by aLIGO, questions have been raised about the frequency of double-compact star/black hole mergers in hierarchical triple star systems, and their gravitational waves, see [56] and references therein. That is only likely to increase the number of studies of gravitational waves emitted from triple star systems.

Mathematics

1) Each of the seven progenitors generates a family of orbits, at different masses and non-vanishing angular momenta, e.g. the Schubart colliding orbit, Ref. [5], generates the

Broucke-Hadjidemetriou-Hénon (BHH), Refs. [6–12], family of collisionless orbits with non-zero angular momenta, that describe the majority of presently known triple-star systems. The remaining six progenitors may now be viewed as credible candidates for observable three-body orbits, provided that their stability persists under changes of mass ratios and of the angular momentum. Those dependences need to be explored in detail. Only the figure-eight orbit has been studied in this regard thus far.

2) Turning the foregoing reasoning around, one can use any new sequence of orbits to argue for the applicability of the Birkhoff-Lewis theorem to its, as yet unknown progenitor. That raises the question of existence of further stable two-dimensional colliding orbits that may generate new sequences of periodic orbits. New periodic orbits can be searched for in different ways, but it is difficult to predict their (in)stability.

3) A remaining mystery is why are the slopes of $T_{s,i} - N_w$ graphs of different sequences so close to each other?

4) Our results form a mathematical conjecture about the applicability of the Birkhoff-Lewis theorem to six/seven progenitor orbits supported by some numerical evidence. One would like to see a definite proof or refutation of this conjecture.

5) Many of the above arguments are generic, so they ought to also hold for periodic three-particle orbits bound by other homogeneous potentials, such as the Coulomb one, [68] or in potentials with other degrees of homogeneity. This conjecture ought to be checked.

6) The task of proving exact periodicity of the here presented numerical orbits remains open; in this regard we follow Feynman [57], and leave that task to mathematicians.

Acknowledgments

V.D. and A.H. thank Aleksandar Bojarov, Marija Janković and Srdjan Marjanović, for their help with setting up the web-site, running the codes on the Zefram cluster and general programming. V.D. was financially supported by the Serbian Ministry of Science and Technological Development under Grants No. OI 171037 and III 41011 and M.S. was supported by the Japan Society for the Promotion of Science (JSPS), Grant-in-Aid for Young Scientists (B) No. 26800059. A.H. was a recipient of the “Dositeja” stipend for the year 2014/2015, from the Fund for Young Talents (Fond za mlade talente - stipendija ”Dositeja”) of the Serbian Ministry for Youth and Sport. The computing cluster Zefram (zefram.ipb.ac.rs) at

the Institute of Physics Belgrade has been extensively used for numerical calculations.

Appendix A: New orbits

1. Preliminaries

a. Nomenclature

Because of the large number of orbits, a nomenclature system had to be invented. New orbits will be named following the pattern S.n.X. α (not to be confused with orbit classes from Refs. [20] and [26]; that notation corresponds to geometric and algebraic symmetries of the orbits.), where:

1. S is the sequence number (roman numeral)
2. n is the smaller of numbers n and \bar{n} (if they are different)
3. $X \in \{A, B, C, \dots\}$ denotes different orbits in case there are more than one with the same n in the same group
4. α or β denotes two different sets of initial conditions for the same solution if they exist at all.

The real-space and shape-sphere orbits of all trajectories can be found on the web site Ref. [25].

b. Some open issues

For some of the new orbits, it is still not completely clear which sequence they should be placed into.

1. Orbits I.5.A, I.8.A, I.11.A and I.14.A (currently in the “butterfly I (n, n)” sequence I) may just as well belong to the “moth (n, n)” sequence VIIb (based on their free group elements of the form $(\mathbf{babABA})^{n+1}\mathbf{B}(\mathbf{abaBAB})^n\mathbf{a}$).
2. Orbits VII.17.A and VII.20.A (currently in the “moth (n, n)” sequence VIIb) may equally well belong to the “butterfly I (n, n)” sequence I (they have the same form $(\mathbf{babABA})^{n+1}\mathbf{B}(\mathbf{abaBAB})^n\mathbf{a}$ of the free group elements as the aforementioned orbits).

3. Orbits IVb.6.A, IVb.9.A, IVb.15.B and IVb.22.A (currently in the “butterfly III $(n, n+1)$ ” sequence IVb) may belong to the “moth III $(n, n+1)$ ” sequence IVc (the first three of these have free group elements of the form $(\mathbf{babABA})^n \mathbf{b}(\mathbf{abaBAB})^n \mathbf{a}$).
4. Orbits IVc.12.B, IVc.13.A, IVc.15.A, IVc.15.B, IVc.15.C, IVc.16.A, IVc.16.B, IVc.16.C, IVc.17.B, IVc.18.A, IVc.21.A and IVc.22.A, currently in the “moth III $(n, n+1)$ ” sequence IVc, may belong to the “butterfly III $(n, n+1)$ ” sequence IVb.

2. Sequence I – butterfly I (n, n)

The orbits in the “butterfly I (n, n) ” sequence have characteristic free group elements

$$(\mathbf{ab})^2(\mathbf{ABAbab})^n(\mathbf{AB})^2(\mathbf{abaBAB})^n,$$

where $n = 1, 2, 3, \dots$. An alternative definition is: free group elements that contain the following sequences of letters $(\mathbf{ab})^2(\mathbf{AB})^2$ or $(\mathbf{ba})^2(\mathbf{BA})^2$ (see Tables VII and VIII).

Setting $n = 0$ in this structure, one finds $(\mathbf{AB})^2(\mathbf{ab})^2$. That is one of the topologies that can be associated with twice the colliding Schubart orbit in the limit of vanishing angular momentum. So, although we list the I.2.A butterfly I as the β orbit in Table VI, we also show the period of the Schubart orbit, for the sake of comparison. The (decent) numerical agreement suggests that the Schubart orbit might be the true progenitor of this sequence.

All the orbits in this sequence have reflection symmetries around two axes – the equator and the meridian that passes through the Euler point. They also have algebraic exchange symmetries of free group elements $(\mathbf{a}, \mathbf{b}) \leftrightarrow (\mathbf{A}, \mathbf{B})$.

Some of these orbits were predicted in Ref. [26], for example I.8.A with $\frac{T}{T_\beta} \approx 4$ and I.12.A with $\frac{T}{T_\beta} \approx 6$. Orbits with odd numbers n were unexpected because all previously known orbits from this sequence had even numbers n .

Linear fit $T|E|^{3/2} = a\left(\frac{n+\bar{n}}{2}\right) + b$ for all orbits from Table VI (excepting v.Schubart’s one) gives $a = 9.957 \pm 0.011$ and $b = -0.2 \pm 0.2$ (see Figure 2.a in the main text).

Ref. [26] also placed the goggles orbit into this sequence. While it does fit in it numerically, it looks completely different both in real space and on the shape-sphere, and its free group element $(\mathbf{ab})^2\mathbf{ABBA}(\mathbf{ba})^2\mathbf{BAAB}$ does not contain the $(\mathbf{ab})^2(\mathbf{AB})^2$ or $(\mathbf{ba})^2(\mathbf{BA})^2$ structure. We have therefore excluded it from this sequence.

Table VI: Orbits in the “butterfly I (n, n)” sequence I: 17 new (denoted by an asterisk) + 2 old (reabeled according to the new naming convention) ones. We also show the period of the colliding Schubart orbit. The second column shows the scale-invariant period $T_{\text{s.i.}} = T|E|^{3/2}$ instead of the period T at energy $E = -0.5$, that was shown in Refs. [20, 21, 24, 26, 29].

Label	$T_{\text{s.i.}}$	$\frac{T_{\text{s.i.}}}{T_{\text{M8}}}$	$\frac{T_{\text{s.i.}}}{T_{\beta}}$	$\frac{N}{N_{\beta}}$	(n, \bar{n})	Old label
I.1.A	4.98307	0.539429	1/4.00004	1/4	1/2,1/2	Schubart
I.2.A	19.9325	2.15774	1	1	2,2	butterfly I
I.2.B	19.9313	2.15762	0.99994	1	2,2	butterfly II
I.5.A	49.6301	5.37257	2.48991	2.5	5,5	*
I.8.A	79.2555	8.57959	3.97619	4	8,8	*
I.9.A	89.5601	9.69509	4.49317	4.5	9,9	*
I.11.A	108.869	11.7853	5.46186	5.5	11,11	*
I.12.A	119.241	12.9081	5.98224	6	12,12	*
I.13.A	129.450	14.0133	6.49442	6.5	13,13	*
I.14.A	138.479	14.9907	6.94740	7	14,14	*
I.16.A	159.167	17.2302	7.98530	8	16,16	*
I.17.A	169.327	18.3300	8.49502	8.5	17,17	*
I.18.A	178.523	19.3255	8.95638	9	18,18	*
I.19.A	188.847	20.4431	9.47433	9.5	19,19	*
I.20.A	199.069	21.5497	9.98716	10	20,20	*
I.21.A	209.198	22.6462	10.4953	10.5	21,21	*
I.22.A	218.506	23.6538	10.9623	11	22,22	*
I.23.A	228.773	24.7652	11.4774	11.5	23,23	*
I.24.A	238.958	25.8678	11.9884	12	24,24	*
I.25.A	249.067	26.9621	12.4955	12.5	25,25	*

Table VII: Non-minimal free group elements of the orbits in the “butterfly I” sequence,
with periods in Table VI.

Label	Free group element
I.1.A	aB
I.2.A	$(ab)^2(AB)^2$
I.2.B	$(ab)^2(AB)^2$
I.5.A	$(ab)^2(ABabab)(AB)^2(abaBAB)$
I.8.A	$(ab)^2(ABabab)^2(AB)^2(abaBAB)^2$
I.9.A	$(ab)^2ABA(ba)^2(BA)^2bab(AB)^2aba(BA)^2(ba)^2BAB$ $= [(ab)^2(AB)^2]b[(ba)^2(BA)^2]A[(ab)^2(AB)^2]B[(ba)^2(BA)^2]^2a$
I.11.A	$(ab)^2(ABabab)^3(AB)^2(abaBAB)^3$
I.12.A	$(ab)^2ABA(ba)^2(BABaba)(BA)^2bab(AB)^2aba(BA)^2(babABA)(ba)^2BAB$
I.13.A	$(ab)^2(AB)^2aba(BA)^2(ba)^2BAB(ab)^2(AB)^2(ab)^2ABA(ba)^2(BA)^2bab(AB)^2$ $= [(ab)^2(AB)^2]^2B[(ba)^2(BA)^2]^2a[(ab)^2(AB)^2]^2b[(ba)^2(BA)^2]A$
I.14.A	$(ab)^2(ABabab)^4(AB)^2(abaBAB)^4$
I.16.A	$[(ab)^2ABA(ba)^2BAB]^2(ab)^2[(AB)^2aba(BA)^2bab]^2(AB)^2$
I.17.A	$(ab)^2(AB)^2aba[(BA)^2(ba)^2]^2BAB(ab)^2(AB)^2(ab)^2ABA[(ba)^2(BA)^2]^2bab(AB)^2$ $= [(ab)^2(AB)^2]^2B[(ba)^2(BA)^2]^3a[(ab)^2(AB)^2]^2b[(ba)^2(BA)^2]^2A$

Table VIII: Non-minimal free group elements of the orbits in the “butterfly I” sequence – continued, periods in Table VI.

Label	Free group element
I.18.A	$(ab)^2(ABababABA)(ba)^2(BABaba)(BA)^2(babABabab)$ $\times (AB)^2(abaBABaba)(BA)^2(babABA)(ba)^2(BABabaBAB)$
I.19.A	$[(ab)^2ABA(ba)^2BAB]^2(ab)^2(ABabab)[(AB)^2aba(BA)^2bab]^2(AB)^2(abaBAB)$
I.20.A	$(ab)^2ABA(ba)^2(BA)^2bab(AB)^2(ab)^2ABA(ba)^2(BA)^2bab$ $\times (AB)^2aba(BA)^2(ba)^2BAB(ab)^2(AB)^2aba(BA)^2(ba)^2BAB$
I.21.A	$[(ab)^2(AB)^2]^2(ab)^2ABA[(ba)^2(BA)^2]^2bab[(AB)^2(ab)^2]^2(AB)^2aba[(BA)^2(ba)^2]^2BAB$ $= [(ab)^2(AB)^2]^3b[(ba)^2(BA)^2]^2A[(ab)^2(AB)^2]^3B[(ba)^2(BA)^2]^3a$
I.22.A	$(ab)^2(ABabab)(AB)^2aba(BA)^2(babABA)(ba)^2BAB(ab)^2(ABabab)$ $\times (AB)^2(abaBAB)(ab)^2ABA(ba)^2(BABaba)(BA)^2bab(AB)^2(abaBAB)$
I.23.A	$[(ab)^2ABA(ba)^2BAB]^2(ab)^2ABA(ba)^2(BA)^2bab[(AB)^2aba(BA)^2bab]^2(AB)^2aba(BA)^2(ba)^2BAB$
I.24.A	$[(ab)^2(AB)^2aba(BA)^2(ba)^2BAB]^2(ab)^2[(AB)^2(ab)^2ABA(ba)^2(BA)^2bab]^2(AB)^2$
I.25.A	$[(ab)^2(AB)^2]^2(ab)^2ABA[(ba)^2(BA)^2]^3bab[(AB)^2(ab)^2]^2(AB)^2aba[(BA)^2(ba)^2]^3BAB$ $= [(ab)^2(AB)^2]^3b[(ba)^2(BA)^2]^3A[(ab)^2(AB)^2]^3B[(ba)^2(BA)^2]^4a$

3. Sequence II – dragonfly (n, n)

Table IX: Orbits in the “dragonfly (n, n) ” sequence II: 14 new (denoted by an asterisk) + 2 old (relabelled according to the new naming convention) ones. We show the period of the “isosceles-orbit”, Ref. [13], for the sake of comparison. The columns are labeled as in

Table VI.

Label	$T_{s.i.}$	$\frac{T_{s.i.}}{T_{Ms}}$	$\frac{T_{s.i.}}{T_{\beta}}$	$\frac{n+\bar{n}}{n_{\beta}+\bar{n}_{\beta}}$	(n, \bar{n})	Old label
II.1.A	9.2	0.99	0.25	1/4	1,1	isosceles
II.2.A	18.4	1.99	0.5	1/2	2,2	?
II.4.A	36.7714	3.98059	1	1	4,4	dragonfly
II.6.A	55.2035	5.97591	1.50126	1.5	6,6	*
II.8.A	73.6540	7.97321	2.00302	2	8,8	*
II.11.A	101.184	10.9534	2.75170	2.75	11,11	bumblebee
II.14.A	128.724	13.9347	3.50066	3.5	14,14	*
II.14.B	128.726	13.9349	3.50071	3.5	14,14	*
II.15.A	137.888	14.9267	3.74987	3.75	15,15	*
II.15.B	137.917	14.9298	3.75066	3.75	15,15	*
II.15.C	137.919	14.9300	3.75071	3.75	15,15	*
II.15.D	138.097	14.9493	3.75555	3.75	15,15	*
II.16.A	147.109	15.9249	4.00064	4	16,16	*
II.16.B	147.163	15.9307	4.00210	4	16,16	*
II.17.A	156.282	16.9179	4.25010	4.25	17,17	*
II.17.B	156.285	16.9182	4.25018	4.25	17,17	*
II.17.C	156.386	16.9291	4.25292	4.25	17,17	*
II.17.D	156.387	16.9293	4.25295	4.25	17,17	*

The “dragonfly (n, n) ” orbits have characteristic free group elements $\mathbf{bA}(\mathbf{baBA})^n\mathbf{aB}(\mathbf{abAB})^n$, where $n = 1, 2, 3 \dots$. An alternative definition is: free group elements that contain \mathbf{A}^2 and \mathbf{B}^2 followed by alternating sequences of letters \mathbf{ab} and \mathbf{AB} (see Table X).

Setting $n = 0$ in this structure, one finds \mathbf{bAaB} , i.e., the (neutral) unit element of the free

group, that corresponds to the trivial topology. That is one of the topologies that can be associated with the colliding “Broucke isosceles orbit”, Ref. [13]: a) $w(\text{isosceles}) = \mathbf{b}^2\mathbf{A}^2$; b) $w(\text{isosceles}) = \mathbf{b}^2\mathbf{a}^2$, and c) $w(\text{isosceles}) = \mathbf{bAaB}$.

So, although we list the II.4.A dragonfly as the β orbit in Table IX, we also show the period of Broucke’s isosceles orbit, for the sake of comparison. The (decent) numerical agreement suggests that the isosceles orbit might be the true progenitor of this sequence.

Orbits II.4.A, II.6.A, II.11.A, II.15.A and II.16.B have reflection symmetries around two axes – the equator and the meridian that passes through the Euler point. All other orbits from this sequence have central reflection symmetry around the Euler point. They also have algebraic exchange symmetries of free group elements; for example II.4.A and II.6.A $(\mathbf{a}, \mathbf{A}) \leftrightarrow (\mathbf{b}, \mathbf{B})$, and II.11.A $(\mathbf{a}, \mathbf{b}) \leftrightarrow (\mathbf{A}, \mathbf{B})$.

Some of these orbits, for example II.6.A with $\frac{T}{T_\beta} \approx \frac{3}{2}$ and II.8.A with $\frac{T}{T_\beta} \approx 2$, were predicted in Ref.[26].

Linear fit $T|E|^{3/2} = a \left(\frac{n+\bar{n}}{2} \right) + b$ for all orbits from Table IX gives $a = 9.194 \pm 0.004$ and $b = 0.04 \pm 0.06$ (see Figure 2.b in the main text). This is the smallest slope value of all the sequences.

Table X: Non-minimal free group elements for orbits in the sequence II – “dragonfly (n, n) ” from Table IX.

Label	Free group element
II.1.A	$\mathbf{bAaB} \simeq \mathbf{b}^2\mathbf{A}^2$
II.2.A	$\mathbf{bA(baBA)aB(abAB)}$
II.4.A	$\mathbf{bA(baBA)^2aB(abAB)^2}$
II.6.A	$\mathbf{bA(baBA)^3aB(abAB)^3}$
II.8.A	$\mathbf{bA(baBA)^5aB(abAB)^3}$
II.11.A	$\mathbf{bA(abAB)^3bA(baBA)^2aB(abAB)^2aB(baBA)^3}$
II.14.A	$\mathbf{a}^2(\mathbf{BAbaBA})\mathbf{b}^2(\mathbf{ABab})^2\mathbf{A}^2(\mathbf{baBA})^2\mathbf{b}^2(\mathbf{ABabAB})\mathbf{a}^2(\mathbf{BAba})^2\mathbf{B}^2(\mathbf{abAB})^2$
II.14.B	$\mathbf{a}^2(\mathbf{BAbaBA})\mathbf{b}^2(\mathbf{ABab})^2\mathbf{A}^2(\mathbf{baBA})^2\mathbf{b}^2(\mathbf{ABabAB})\mathbf{a}^2(\mathbf{BAba})^2\mathbf{B}^2(\mathbf{abAB})^2$
II.15.A	$\mathbf{b}^2(\mathbf{ABabAB})\mathbf{a}^2(\mathbf{BAbaBA})\mathbf{b}^2(\mathbf{ABabAB})\mathbf{a}^2(\mathbf{BAba})\mathbf{B}^2(\mathbf{abABab})\mathbf{A}^2(\mathbf{baBAba})\mathbf{B}^2(\mathbf{abABab})\mathbf{A}^2(\mathbf{baBA})$
II.15.B	$\mathbf{b}^2(\mathbf{ABabABabAB})\mathbf{a}^2(\mathbf{BAbaBA})\mathbf{b}^2(\mathbf{ABabABabAB})\mathbf{a}^2(\mathbf{BAba})^2\mathbf{B}^2(\mathbf{abABab})\mathbf{A}^2(\mathbf{baBA})^2$
II.15.C	$\mathbf{A}^2(\mathbf{baBAbaBAba})\mathbf{B}^2(\mathbf{abABab})\mathbf{A}^2(\mathbf{baBAbaBAba})\mathbf{B}^2(\mathbf{abAB})^2\mathbf{a}^2(\mathbf{BAbaBA})\mathbf{b}^2(\mathbf{ABab})^2$
II.15.D	$\mathbf{A}^2(\mathbf{baBAbaBAba})\mathbf{B}^2(\mathbf{abAB})^3\mathbf{a}^2(\mathbf{BAbaBAbaBAbaBAbaBA})\mathbf{b}^2(\mathbf{ABab})^3$
II.16.A	$\mathbf{a}^2(\mathbf{BAbaBA})\mathbf{b}^2(\mathbf{ABabAB})\mathbf{a}^2(\mathbf{BAbaBA})\mathbf{b}^2(\mathbf{ABabABabABabAB})\mathbf{a}^2(\mathbf{BAbaBA})\mathbf{b}^2(\mathbf{ABabABabABabAB})$
II.16.B	$\mathbf{A}^2(\mathbf{baBAbaBAba})\mathbf{B}^2(\mathbf{abAB})^2\mathbf{a}^2(\mathbf{BAba})^2\mathbf{B}^2(\mathbf{abABabABab})\mathbf{A}^2(\mathbf{baBA})^2\mathbf{b}^2(\mathbf{ABab})^2$
II.17.A	$\mathbf{b}^2(\mathbf{ABabAB})\mathbf{a}^2(\mathbf{BAbaBA})\mathbf{b}^2(\mathbf{ABabAB})\mathbf{a}^2(\mathbf{BAba})^2\mathbf{B}^2(\mathbf{abABab})\mathbf{A}^2(\mathbf{baBAba})\mathbf{B}^2(\mathbf{abABab})\mathbf{A}^2(\mathbf{baBA})^2$
II.17.B	$\mathbf{b}^2(\mathbf{ABabAB})\mathbf{a}^2(\mathbf{BAbaBA})\mathbf{b}^2(\mathbf{ABabAB})\mathbf{a}^2(\mathbf{BAba})^2\mathbf{B}^2(\mathbf{abABab})\mathbf{A}^2(\mathbf{baBAba})\mathbf{B}^2(\mathbf{abABab})\mathbf{A}^2(\mathbf{baBA})^2$
II.17.C	$\mathbf{b}^2(\mathbf{ABabABabAB})\mathbf{a}^2(\mathbf{BAba})^2\mathbf{B}^2(\mathbf{abABabABab})\mathbf{A}^2(\mathbf{baBAbaBAba})\mathbf{B}^2(\mathbf{abABabABab})\mathbf{A}^2(\mathbf{baBA})^2$
II.17.D	$\mathbf{A}^2(\mathbf{baBAbaBAba})\mathbf{B}^2(\mathbf{abAB})^2\mathbf{a}^2(\mathbf{BAbaBAbaBA})\mathbf{b}^2(\mathbf{ABabABabAB})\mathbf{a}^2(\mathbf{BAbaBAbaBA})\mathbf{b}^2(\mathbf{ABab})^2$

4. Sequence III – yin-yang (n, n)

The “yin-yang (n, n) ” orbits have characteristic free group elements $(\mathbf{abaBAB})^n\mathbf{a}(\mathbf{babABA})^n\mathbf{A}$, where $n = 1, 2, 3, \dots$, (see Table XII).

When one sets $n = 0$ in this structure, one finds $\mathbf{bB} = \mathbf{e}$, i.e., the (neutral) unit element of the free group, that corresponds to the trivial topology. This is one of the topologies that can be associated with the colliding “S-orbit”, Ref. [22]: 1) $w(\mathbf{S} - \text{orbit}) = \mathbf{abaABA}$, 2) $w(\mathbf{S} - \text{orbit}) = \mathbf{ababAB} = (\mathbf{ab})^2\mathbf{AB}$.

Table XI: Orbits in the “yin-yang (n, n) ” sequence III: 9 new (denoted by an asterisk) + 2 old (reabeled according to the new naming convention) ones. We show the period of the “S-orbit”, Ref. [22, 23], for the sake of comparison. Columns are the same as in Table VI.

Label	$T_{\text{s.i.}}$	$\frac{T_{\text{s.i.}}}{T_{\text{M8}}}$	$\frac{T_{\text{s.i.}}}{T_{\beta}}$	$\frac{n+\bar{n}}{n_{\beta}+\bar{n}_{\beta}}$	(n, \bar{n})	Old label
III.1.A	14.8	1.6	0.5	$\frac{1}{2}$	2,1	S-orbit
III.3.A	29.6021	3.20450	1	1	3,3	yin-yang Ia
III.9.A	88.8065	9.61351	3.000 007	3	9,9	*
III.12.A	118.396	12.8166	3.999 581	4	12,12	yin-yang IIa
III.15.A	147.998	16.0211	4.999 578	5	15,15	*
III.15.B	148.010	16.0224	4.999 983	5	15,15	*
III.15.C	148.010	16.0224	4.999 983	5	15,15	*
III.18.A	177.602	19.2258	5.999 642	6	18,18	*
III.21.A	207.207	22.4306	6.999 740	7	21,21	*
III.13.A	133.196	14.4188	4.499 546	4.5	13,14	*
III.16.A	162.801	17.6236	5.499 644	5.5	16,17	*
III.19.A	192.398	20.8275	6.499 471	6.5	19,20	*

Setting $n = 1$ in this structure, one finds $(\text{abaBAB})\mathbf{a}(\text{babABA})\mathbf{A}$, i.e., the free group element of the III.3.A yin-yang I orbit. So, although we list the III.3.A yin-yang I as the β orbit in Table XI, we also show the period of the S-orbit, for the sake of comparison. The (decent) numerical agreement suggests that the S-orbit might be the true progenitor of this sequence.

Orbit III.9.A is a satellite of orbit III.3.A with $k = 3$. Its value of $T|E|^{3/2}$ is three times the value for its apparent progenitor orbit, to the precision of $7 \cdot 10^{-6}$. Similarly, orbits III.15.B and III.15.C are both $k = 5$ satellites of orbit III.3.A. These are three new satellite-progenitor pairs of orbits, the first after the moth I - yarn pair and the figure-eight satellites.

All the orbits from this sequence have central reflection symmetry around the Euler point. They have no algebraic exchange symmetries of free group elements.

Orbits III.9.A with $\frac{T}{T_{\beta}} \approx 3$, III.15.A with $\frac{T}{T_{\beta}} \approx 5$, III.18.A with $\frac{T}{T_{\beta}} \approx 6$ and III.21.A with

$\frac{T}{T_\beta} \approx 7$ were predicted in Ref. [26]. Orbits III.13.A with $\frac{T}{T_\beta} \approx 4.5$, III.16.A with $\frac{T}{T_\beta} \approx 5.5$ and III.19.A with $\frac{T}{T_\beta} \approx 6.5$ were unexpected, because they have different numbers n and \bar{n} unlike the previously known orbits.

Linear fit $T|E|^{3/2} = a \left(\frac{n+\bar{n}}{2} \right) + b$ for all orbits from Table XI (except for the S-orbit) gives $a = 9.8667 \pm 0.0003$ and $b = 0.002 \pm 0.004$ (see Figure 2.c in the main text).

Table XII: Non-minimal free group elements for the orbits in the sequence III – “yin-yang (n, n) ”, from Table XI.

Label	Free group element
III.1.A	$\text{abaABA} \simeq (\text{ab})^2 \text{AB}$
III.3.A	$(\text{abaBAB})\text{a}(\text{babABA})\text{A}$
III.9.A	$[(\text{abaBAB})\text{a}(\text{babABA})\text{A}]^3$
III.12.A	$(\text{abaBAB})^4 \text{b}(\text{babABA})^4 \text{B}$
III.15.A	$(\text{abaBAB})^5 \text{b}(\text{babABA})^5 \text{B}$
III.15.B	$[(\text{abaBAB})\text{a}(\text{babABA})\text{A}]^5$
III.15.C	$[(\text{abaBAB})\text{a}(\text{babABA})\text{A}]^5$
III.18.A	$(\text{abaBAB})^6 \text{b}(\text{babABA})^6 \text{B}$
III.21.A	$(\text{abaBAB})^7 \text{a}(\text{babABA})^7 \text{A}$
III.13.A	$(\text{abaBAB})^5 \text{A}(\text{babABA})^4 \text{A}$
III.16.A	$(\text{abaBAB})^6 \text{A}(\text{babABA})^5 \text{A}$
III.19.A	$(\text{abaBAB})^6 \text{a}(\text{babABA})^7 \text{a}$

5. Sequence IVa – moth I $(n, n+1)$

The “moth I $(n, n+1)$ ” sequence and the following two (IVb and IVc) were a part of a larger sequence of orbits (“moth I, II, III - butterfly III”) in Ref. [26]. Here they are divided into three parts, based on the slope of their $T|E|^{3/2} \left(\frac{n+\bar{n}}{2} \right)$ linear dependence, the appearance of their trajectories in real and shape-space, and the patterns in the words that define their topology.

Table XIII: Orbits in the “moth I $(n, n + 1)$ ” sequence IVa: 16 new (denoted by an asterisk) + 2 old (relabelled according to the new naming convention) ones. We show the period of the Schubart orbit, for the sake of comparison. Columns are the same as in Table VI.

Label	$T_{s.i.}$	$\frac{T_{s.i.}}{T_{Ms}}$	$\frac{T_{s.i.}}{T_{\beta}}$	$\frac{n+\bar{n}}{n_{\beta}+\bar{n}_{\beta}}$	(n, \bar{n})	Old label
IVa.0.A	4.98307	0.539429	1/4.85757	1/5	0,1	Schubart
IVa.2.A	24.2056	2.62031	1	1	2,3	moth I
IVa.4.A	42.7821	4.63126	1.76745	1.8	4,5	moth II
IVa.4.B	42.7833	4.63139	1.76750	1.8	4,5	*
IVa.6.A	61.2901	6.63479	2.53206	2.6	6,7	*
IVa.8.A	79.7665	8.63491	3.29537	3.4	8,9	*
IVa.8.B	79.7670	8.63496	3.29539	3.4	8,9	*
IVa.8.C	79.7671	8.63497	3.29540	3.4	8,9	*
IVa.8.D	79.7757	8.63590	3.29575	3.4	8,9	*
IVa.8.E	79.7758	8.63591	3.29576	3.4	8,9	*
IVa.8.F	79.7794	8.63630	3.29591	3.4	8,9	*
IVa.8.G	79.7794	8.63630	3.29591	3.4	8,9	*
IVa.8.H	79.7794	8.63630	3.29591	3.4	8,9	*
IVa.8.I	81.9508	8.87136	3.38561	3.4	8,9	*
IVa.8.J	79.7766	8.63600	3.29579	3.4	8,9	*
IVa.9.A	89.0213	9.63676	3.67772	3.8	9,10	*
IVa.9.B	91.2445	9.87743	3.76956	3.8	9,10	*
IVa.10.A	98.2622	10.6371	4.05948	4.2	10,11	*
IVa.10.B	100.524	10.8820	4.15292	4.2	10,11	*

These orbits have characteristic free group elements $(abAB)^n A (baBA)^n B$, where $n = 1, 2, 3, \dots$, (see Tables XV, XVI).

When one sets $n = 0$ in this structure, one finds AB , i.e., one of two topologies that turn into the Schubart orbit in the limit of vanishing angular momentum. So, although we take the IVa.2.A moth I as the β orbit in Tables XIII and XIV, we also show the period of the

Table XIV: Orbits in the “moth I ($n, n + 1$)” sequence IVa – continued: 19 new (denoted by an asterisk). Columns are the same as in Table VI.

Label	$T_{s.i.}$	$\frac{T_{s.i.}}{T_{M8}}$	$\frac{T_{s.i.}}{T_{\beta}}$	$\frac{n+\bar{n}}{n_{\beta}+\bar{n}_{\beta}}$	(n, \bar{n})	Old label
IVa.11.A. α	107.502	11.6373	4.44120	4.6	11,12	*
IVa.11.A. β	107.502	11.6373	4.44120	4.6	11,12	*
IVa.11.B	107.502	11.6373	4.44120	4.6	11,12	*
IVa.12.A	116.733	12.6366	4.82256	5	12,13	*
IVa.12.B	116.741	12.6375	4.82289	5	12,13	*
IVa.12.C	116.742	12.6376	4.82293	5	12,13	*
IVa.12.D	119.074	12.8900	4.91927	5	12,13	*
IVa.12.E	121.028	13.1016	5.00000	5	12,13	*
IVa.13.A	125.975	13.6371	5.20437	5.4	13,14	*
IVa.13.B	125.981	13.6377	5.20462	5.4	13,14	*
IVa.13.C	125.989	13.6386	5.20495	5.4	13,14	*
IVa.14.A	135.219	14.6378	5.58627	5.8	14,15	*
IVa.14.B	135.220	14.6379	5.58631	5.8	14,15	*
IVa.14.C	137.607	14.8963	5.68492	5.8	14,15	*
IVa.14.D	137.607	14.8963	5.68492	5.8	14,15	*
IVa.15.A	144.456	15.6377	5.96788	6.2	15,16	*
IVa.15.B	146.864	15.8984	6.06736	6.2	15,16	*
IVa.8.K	85.5569	9.26173	3.53459	3.6	8,10	*
IVa.16.A	159.549	17.2715	6.59141	6.8	16,18	*

Schubart orbit, for the sake of comparison. The (decent) numerical agreement suggests that the Schubart orbit might be the true progenitor of this sequence.

Orbits IVa.2.A, IVa.4.A, IVa.6.A, IVa.8.B, IVa.8.G, IVa.9.B, IVa.10.A, IVa.12.A, IVa.12.C, IVa.14.A and IVa.15.B have reflection symmetries around two axes – the equator and the meridian that passes through the Euler point. All other orbits from this sequence have central reflection symmetry around the Euler point.

Orbits IVa.8.A and IVa.8.C are mirror images of each other on the shape sphere. They have the same topology as the symmetric orbit IVa.8.B. Similar situation is encountered again with mirror images IVa.8.F and IVa.8.H, and symmetric IVa.8.G with the same topology.

Most of these orbits have algebraic exchange symmetries of free group elements $(\mathbf{a}, \mathbf{A}) \leftrightarrow (\mathbf{b}, \mathbf{B})$.

Orbit IVa.8.K is a $k = 2$ satellite orbit of moth II (IVa.4.A). However, its value of $T|E|^{3/2}$ is not exactly two times larger than the value for moth II (difference is of the order 10^{-1}), and it looks completely different from the other orbits in this sequence, both in real and in shape space. Despite its topology, perhaps this orbit does not belong into this sequence.

Linear fit $T|E|^{3/2} = a \left(\frac{n+\bar{n}}{2} \right) + b$ for all orbits from Tables XIII and XIV gives $a = 9.34 \pm 0.06$ and $b = 0.7 \pm 0.7$ (see Figure 2.d in the main text).

Several orbits with same values of $\frac{n+\bar{n}}{2}$ have significantly different values of $T|E|^{3/2}$, see Figure 2.d in the main text and Tables XIII and XIV. This suggests that the IVa - moth I sequence might perhaps be further divided into two or more subsequences. One possible division, shown below, is based on both topology and appearance of orbits in real space.

- Sequence IVa1: IVa.2.A, IVa.4.A, IVa.4.B, IVa.6.A, IVa.8.A, IVa.8.B, IVa.8.C, IVa.8.D, IVa.8.E, IVa.8.F, IVa.8.G, IVa.8.H, IVa.8.J, IVa.9.A, IVa.10.A, IVa.11.A, IVa.11.B, IVa.12.A, IVa.12.B, IVa.12.C, IVa.13.A, IVa.13.B, IVa.13.C, IVa.14.A, IVa.14.B, IVa.15.A.
- Sequence IVa2: IVa.8.I, IVa.9.B, IVa.10.B, IVa.12.D, IVa.14.C, IVa.14.D, IVa.15.B.
- Moth II satellite: IVa.8.K.
- Other: IVa.12.E, IVa.16.A.

Sequence IVa1 orbits (except IVa.8.A, IVa.8.B and IVa.8.C) resemble moth I and moth II in real space, while sequence IVa2 orbits (except IVa.14.C and IVa.14.D) look completely different. Also, sequence IVa1 orbits have free group elements of the form $(\mathbf{abAB})^n \mathbf{a}(\mathbf{baBA})^m \mathbf{b}$, where n and m are some integers. Free group elements of sequence IVa2 orbits are products of several sequence IVa1 elements. All orbits in sequence IVa1 have algebraic exchange symmetries of free group elements $(\mathbf{a}, \mathbf{A}) \leftrightarrow (\mathbf{b}, \mathbf{B})$.

Table XV: Non-minimal free group elements for the orbits from the “moth I $(n, n + 1)$ ” sequence IVa, periods from Table XIII. Columns are the same as in Table VI.

Label	Free group element
IVa.0.A	AB
IVa.2.A	$(abAB)A(baBA)B$
IVa.4.A	$(abAB)^2A(baBA)^2B$
IVa.4.B	$(abAB)^2a(baBA)^2b$
IVa.6.A	$(abAB)^3A(baBA)^3B$
IVa.8.A	$(abAB)^4a(baBA)^4b$
IVa.8.B	$(abAB)^4a(baBA)^4b$
IVa.8.C	$(abAB)^4a(baBA)^4b$
IVa.8.D	$(abAB)^3A(baBA)^5B$
IVa.8.E	$(abAB)^3A(baBA)^5B$
IVa.8.F	$(abAB)^4A(baBA)^4B$
IVa.8.G	$(abAB)^4A(baBA)^4B$
IVa.8.H	$(abAB)^4A(baBA)^4B$
IVa.8.I	$[(abAB)a(baBA)b]^2[(abAB)^2A(baBA)B]$
IVa.8.J	$(abAB)^5A(baBA)^3B$
IVa.9.A	$(abAB)^4A(baBA)^5B$
IVa.9.B	$[(abAB)^2A(baBA)B][(abAB)a(baBA)^2B][(abAB)A(baBA)b]$
IVa.10.A	$(abAB)^5A(baBA)^5B$
IVa.10.B	$[(abAB)a(baBA)^2B][(abAB)^2A(baBA)b][(abAB)^2A(baBA)B]$

Table XVI: Non-minimal free group elements for the orbits from the “moth I $(n, n + 1)$ ” sequence IVa – continued, periods from Table XIV. Columns are the same as in Table VI.

Label	Free group element
IVa.11.A. α	$(abAB)^5a(baBA)^6b$
IVa.11.A. β	$(abAB)^6A(baBA)^5B$
IVa.11.B	$(abAB)^6A(baBA)^4B$
IVa.12.A	$(abAB)^6A(baBA)^5B$
IVa.12.B	$(abAB)^5A(baBA)^7B$
IVa.12.C	$(abAB)^6a(baBA)^6b$
IVa.12.D	$[(abAB)a(baBA)^3B][(abAB)a(baBA)^3b][(abAB)^2A(baBA)B]$
IVa.12.E	$[(abAB)^2A(baBA)B][(abAB)A(baBA)B]$ $\times [(abAB)a(baBA)b][(abAB)A(baBA)B]a(baBA)b$
IVa.13.A	$(abAB)^6A(baBA)^7B$
IVa.13.B	$(abAB)^6A(baBA)^7B$
IVa.13.C	$(abAB)^7a(baBA)^6b$
IVa.14.A	$(abAB)^7A(baBA)^7B$
IVa.14.B	$(abAB)^7A(baBA)^7B$
IVa.14.C	$[(abAB)^3A(baBA)^2B][(abAB)^2A(baBA)^2B]^2$
IVa.14.D	$[(abAB)^3A(baBA)^2B][(abAB)^2a(baBA)^2b]^2$
IVa.15.A	$(abAB)^{10}A(baBA)^5B$
IVa.15.B	$[(abAB)^3A(baBA)^2b][(abAB)^2a(baBA)^3B][(abAB)^2a(baBA)^2b]$
IVa.8.K	$[(abAB)^2a(baBA)^2b]^2$
IVa.16.A	$[(abAB)^4A(baBA)^5B][(abAB)^4A(baBA)^3B]$

6. Sequence IVb – butterfly III $(n, n + 1)$

Table XVII: Orbits in the “butterfly III $(n, n + 1)$ ” sequence IVb: 18 new (denoted by an asterisk) + 1 old (reabeled according to the new naming convention). We show the period of the Schubart orbit, for the sake of comparison. Columns are the same as in Table VI.

Label	$T_{s.i.}$	$\frac{T_{s.i.}}{T_{M8}}$	$\frac{T_{s.i.}}{T_{\beta}}$	$\frac{n+\bar{n}}{n_{\beta}+\bar{n}_{\beta}}$	(n, \bar{n})	Old label
IVb.0.A	4.98307	0.539429	1/6.98409	1/7	0,1	Schubart
IVb.3.A	34.8022	3.7674	1	1	3,4	butterfly III
IVb.6.A	64.4455	6.97637	1.85177	1.85714	6,7	*
IVb.7.A	74.6945	8.08585	2.14626	2.14286	7,8	*
IVb.9.A	94.0628	10.1825	2.70278	2.71429	9,10	*
IVb.11.A	114.567	12.4021	3.29195	3.28571	11,12	*
IVb.14.A	144.315	15.6224	4.14672	4.14286	14,15	*
IVb.14.B	144.314	15.6223	4.14669	4.14286	14,15	*
IVb.15.A	153.282	16.5931	4.40438	4.42857	15,16	*
IVb.15.B	153.282	16.5931	4.40438	4.42857	15,16	*
IVb.15.C. α	154.045	16.6757	4.42630	4.42857	15,16	*
IVb.15.C. β	154.045	16.6757	4.42630	4.42857	15,16	*
IVb.15.D	154.433	16.7177	4.43745	4.42857	15,16	*
IVb.15.E	154.436	16.7181	4.43754	4.42857	15,16	*
IVb.15.F	154.432	16.7176	4.43742	4.42857	15,16	*
IVb.18.A	184.204	19.9405	5.29288	5.28571	18,19	*
IVb.18.B	184.206	19.9407	5.29294	5.28571	18,19	*
IVb.15.G	174.013	18.8373	8.73011	8.75	15,20	*
IVb.15.H	174.014	18.8374	8.73016	8.75	15,20	*
IVb.17.A	184.207	19.9408	9.24154	9.25	17,20	*

The “butterfly III $(n, n + 1)$ ” orbits have characteristic free group elements $[(ab)^2(AB)^2]^n b[(ba)^2(BA)^2]^n a$, where $n = 1, 2, 3, \dots$, (see Tables XIX, XX). They are in fact very similar to the sequence I (butterfly I) orbits; the only difference is that in this case

Table XVIII: Orbits in the “butterfly III ($n, n + 1$)” sequence IVb – continued: 12 new (denoted by an asterisk) + 1 old (reabeled according to the new naming convention).

Columns are the same as in Table VI.

Label	$T_{s.i.}$	$\frac{T_{s.i.}}{T_{MS}}$	$\frac{T_{s.i.}}{T_{\beta}}$	$\frac{n+\bar{n}}{n_{\beta}+\bar{n}_{\beta}}$	(n, \bar{n})	Old label
IVb.19.A	194.299	21.0333	5.58295	5.57143	19,20	*
IVb.20.A	203.679	22.0487	5.85247	5.85714	20,21	*
IVb.21.A	213.925	23.1579	6.14688	6.14286	21,22	*
IVb.22.A	222.964	24.1364	6.40661	6.42857	22,23	*
IVb.22.B	224.090	24.2583	6.43896	6.42857	22,23	*
IVb.23.A	233.329	25.2584	6.70443	6.71429	23,24	*
IVb.23.B	234.165	25.3489	6.72845	6.71429	23,24	*
IVb.23.C	234.164	25.3488	6.72843	6.71429	23,24	*
IVb.23.D	234.169	25.3493	6.72857	6.71429	23,24	*
IVb.24.A	244.172	26.4322	7.01599	7	24,25	butterfly IV
IVb.25.A	253.823	27.4769	7.29330	7.28571	25,26	*
IVb.26.A	263.958	28.5741	7.58452	7.57143	26,27	*
IVb.27.A	274.027	29.6640	7.87384	7.85714	27,28	*

$\bar{n} = n + 1$ instead of $\bar{n} = n$.

When one sets $n = 0$ in this structure, one finds AB, i.e., one of two topologies that turn into the Schubart orbit in the limit of vanishing angular momentum. So, although we took the IVb.3.A butterfly III as the progenitor orbit in Tables XVII and XVIII, we also show the period of the Schubart orbit, for the sake of comparison. The (decent) numerical agreement suggests that the Schubart orbit might be the true progenitor of this sequence.

Most of the orbits in this sequence have reflection symmetries around two axes – the equator and the meridian that passes through the Euler point. These orbits also have algebraic exchange symmetries of free group elements $(a, b) \leftrightarrow (A, B)$. Exceptions are IVb.15.C. α , IVb.15.C. β , IVb.15.G, IVb.15.H IVb.23.B and IVb.23.D; these orbits have central reflection symmetry about the Euler point.

Some of these orbit look different from the others; their shapes seem less regular

(IVb.15.C. α , IVb.15.C. β , IVb.15.G, IVb.15.H, IVb.17.A, IVb.18.B, IVb.22.A, IVb.22.B, IVb.23.B and IVb.23.D). However, their free group elements follow the same pattern as others in this sequence.

Orbits IVb.15.G and IVb.15.H with $\bar{n} = n + 5$ and IVb.17.A with $\bar{n} = n + 3$ were also added to this sequence. Two of those orbits, IVb.15.G and IVb.15.H, are $k = 5$ satellite orbits of butterfly III (IVb.3.A). These two orbits are also mirror images of each other on the shape sphere.

Linear fit $T|E|^{3/2} = a \left(\frac{n+\bar{n}}{2} \right) + b$ for all orbits from Tables XVII and XVIII gives $a = 9.967 \pm 0.012$ and $b = -0.3 \pm 0.3$ (see Figure 2.e in the main text).

This value of the slope parameter a coincides with the value of the same parameter for group I - butterfly I, within the stated absolute errors. That suggest that these two groups may belong to the same sequence, in spite of differences (equal – different) in values of n and \bar{n} .

Table XIX: Non-minimal free group elements for the orbits from the “butterfly III
 $(n, n + 1)$ ” sequence IVb, periods from Table XVII.

Label	Free group element
IVb.0.A	BA
IVb.3.A	$[(ab)^2(AB)^2]B[(ba)^2(BA)^2]A$
IVb.6.A	$[(ab)^2(AB)^2]bA[(ab)^2(AB)^2]b[(ba)^2(BA)^2]aB[(ba)^2(BA)^2]a$
IVb.7.A	$[(ab)^2(AB)^2]^2B[(ba)^2(BA)^2]^2A$
IVb.9.A	$\{[(ab)^2(AB)^2]bA\}^2[(ab)^2(AB)^2]b\{[(ba)^2(BA)^2]aB\}^2[(ba)^2(BA)^2]a$
IVb.11.A	$[(ab)^2(AB)^2]^3a[(ba)^2(BA)^2]^3b$
IVb.14.A	$[(ab)^2(AB)^2]b[(ba)^2(BA)^2]A[(ab)^2(AB)^2]^2b$ $\times [(ba)^2(BA)^2]a[(ab)^2(AB)^2]B[(ba)^2(BA)^2]^2a$
IVb.14.B	$[(ab)^2(AB)^2]b[(ba)^2(BA)^2]A[(ab)^2(AB)^2]^2b$ $\times [(ba)^2(BA)^2]a[(ab)^2(AB)^2]B[(ba)^2(BA)^2]^2a$
IVb.15.A	$\{[(ab)^2(AB)^2]bA\}^4[(ab)^2(AB)^2]b\{[(ba)^2(BA)^2]aB\}^4[(ba)^2(BA)^2]a$
IVb.15.B	$\{[(ab)^2(AB)^2]bA\}^4[(ab)^2(AB)^2]b\{[(ba)^2(BA)^2]aB\}^4[(ba)^2(BA)^2]a$
IVb.15.C. α	$[(ab)^2(AB)^2]b[(ba)^2(BA)^2]aB[(ba)^2(BA)^2]A$ $\times \{[(ab)^2(AB)^2]B[(ba)^2(BA)^2]A\}^2[(ab)^2(AB)^2]b[(ba)^2(BA)^2]a$
IVb.15.C. β	$\{[(ab)^2(AB)^2]b[(ba)^2(BA)^2]a\}^2[(ab)^2(AB)^2]bA$ $\times [(ab)^2(AB)^2]B[(ba)^2(BA)^2]A[(ab)^2(AB)^2]B[(ba)^2(BA)^2]a$
IVb.15.D	$[(ab)^2(AB)^2]^4B[(ba)^2(BA)^2]^4A$
IVb.15.E	$[(ab)^2(AB)^2]^4B[(ba)^2(BA)^2]^4A$
IVb.15.F	$[(ab)^2(AB)^2]^4B[(ba)^2(BA)^2]^4A$
IVb.15.G	$\{[(ab)^2(AB)^2]b[(ba)^2(BA)^2]a\}^5$
IVb.15.H	$\{[(ab)^2(AB)^2]b[(ba)^2(BA)^2]a\}^5$
IVb.17.A	$[(ab)^2(AB)^2]b[(ba)^2(BA)^2]^2a[(ab)^2(AB)^2]^2b$ $\times [(ba)^2(BA)^2]a[(ab)^2(AB)^2]^2b[(ba)^2(BA)^2]^2a$
IVb.18.A	$[(ab)^2(AB)^2]^2B[(ba)^2(BA)^2]^2a[(ab)^2(AB)^2]B$ $\times [(ba)^2(BA)^2]^2A[(ab)^2(AB)^2]^2b[(ba)^2(BA)^2]A$
IVb.18.B	$[(ab)^2(AB)^2]^2B[(ba)^2(BA)^2]^2a[(ab)^2(AB)^2]B$ $\times [(ba)^2(BA)^2]^2A[(ab)^2(AB)^2]^2b[(ba)^2(BA)^2]A$

Table XX: Non-minimal free group elements for the orbits from the “butterfly III
 $(n, n + 1)$ ” sequence IVb – continued, periods from Table XVIII.

Label	Free group element
IVb.19.A	$[(ab)^2(AB)^2]^5b[(ba)^2(BA)^2]^5a$
IVb.20.A	$\{[(ab)^2(AB)^2]b[(ba)^2(BA)^2]a\}^2B[(ba)^2(BA)^2]A[(ab)^2(AB)^2]B$ $\times \{[(ba)^2(BA)^2]a[(ab)^2(AB)^2]b\}^2A[(ab)^2(AB)^2]B[(ba)^2(BA)^2]A$
IVb.21.A	$[(ab)^2(AB)^2]b[(ba)^2(BA)^2]A$ $\times [(ab)^2(AB)^2]B[(ba)^2(BA)^2]A[(ab)^2(AB)^2]^2b$ $\times [(ba)^2(BA)^2]a[(ab)^2(AB)^2]B[(ba)^2(BA)^2]A$ $\times [(ab)^2(AB)^2]B[(ba)^2(BA)^2]^2a$
IVb.22.A	$\{[(ab)^2(AB)^2]bA\}^2[(ab)^2(AB)^2]B[(ba)^2(BA)^2]aB$ $\times [(ba)^2(BA)^2]A[(ab)^2(AB)^2]bA[(ab)^2(AB)^2]b$ $\times \{[(ba)^2(BA)^2]aB\}^2[(ba)^2(BA)^2]A[(ab)^2(AB)^2]bA$ $\times [(ab)^2(AB)^2]B[(ba)^2(BA)^2]aB[(ba)^2(BA)^2]a$
IVb.22.B	$[(ab)^2(AB)^2]^3b[(ba)^2(BA)^2]A[(ab)^2(AB)^2]^2b$ $\times [(ba)^2(BA)^2]^3a[(ab)^2(AB)^2]B[(ba)^2(BA)^2]^2a$
IVb.23.A	$\{[(ab)^2(AB)^2]bA[(ab)^2(AB)^2]B[(ba)^2(BA)^2]a\}^2$ $\times \{[(ab)^2(AB)^2]b[(ba)^2(BA)^2]aB[(ba)^2(BA)^2]A\}^2$ $\times [(ab)^2(AB)^2]b[(ba)^2(BA)^2]a$
IVb.23.B	$[(ab)^2(AB)^2]^4B[(ba)^2(BA)^2]^8A$
IVb.23.C	$[(ab)^2(AB)^2]^6B[(ba)^2(BA)^2]^6A$
IVb.23.D	$[(ab)^2(AB)^2]^8B[(ba)^2(BA)^2]^4A$
IVb.24.A	$[(ab)^2(AB)^2]^6A[(ba)^2(BA)^2]^6B$
IVb.25.A	$[(ab)^2(AB)^2]b[(ba)^2(BA)^2]A[(ab)^2(AB)^2]^2b$ $\times [(ba)^2(BA)^2]A[(ab)^2(AB)^2]^2b$ $\times [(ba)^2(BA)^2]a[(ab)^2(AB)^2]B$ $\times [(ba)^2(BA)^2]^2a[(ab)^2(AB)^2]B[(ba)^2(BA)^2]^2a$
IVb.26.A	$[(ab)^2(AB)^2]^2B[(ba)^2(BA)^2]^3a[(ab)^2(AB)^2]^2B$ $\times [(ba)^2(BA)^2]^2A[(ab)^2(AB)^2]^3b[(ba)^2(BA)^2]^2A$
IVb.27.A	$[(ab)^2(AB)^2]^7b[(ba)^2(BA)^2]^7a$

7. Sequence IVc – moth III $(n, n + 1)$

The “moth III $(n, n + 1)$ ” orbits have characteristic free group elements $(babABA)^n A (abaBAB)^n B$, where $n = 1, 2, 3, \dots$, (see Table XXII).

When one sets $n = 0$ in this structure, one obtains AB, i.e., one of two topologies that turn into the Schubart orbit in the limit of vanishing angular momentum. So, although we take the IVc.5.A as the β orbit, in Table XXI we also show the period of the Schubart orbit, for the sake of comparison, as well as one prediction: the IVc.2.A orbit that ought to exist, but has not been found, as yet. The (decent) numerical agreement suggests that the Schubart orbit might be the true progenitor of this sequence.

Orbits IVc.5.A, IVc.12.B, IVc.13.A, IVc.15.A, IVc.15.B, IVc.15.C, IVc.16.A, IVc.16.B, IVc.16.C, IVc.17.A, IVc.18.A, IVc.19.A, IVc.21.A and IVc.22.A have reflection symmetries around two axes – the equator and the meridian that passes through the Euler point. Orbits IVc.8.A, IVc.8.B, IVc.12.A, IVc.19.B. α and IVc.19.B. β have central reflection symmetry around the Euler point.

Orbits IVc.5.A, IVc.12.B, IVc.15.A, IVc.17.A, IVc.18.A and IVc.21.A also have algebraic exchange symmetries of free group elements $(a, A) \leftrightarrow (b, B)$.

Orbits IVc.8.A, IVc.8.B, IVc.19.B. α and IVc.19.B. β $\bar{n} = n + 2$ were also added to this sequence.

Linear fit $T|E|^{3/2} = a \left(\frac{n+\bar{n}}{2} \right) + b$ for all orbits from Table XXI gives $a = 9.94 \pm 0.04$ and $b = -1.2 \pm 0.7$ (see Figure 2.f in the main text). This agrees, within stated errors, with sequence IVb butterfly III (n, n) .

Table XXI: Orbits in the “moth III ($n, n + 1$)” sequence IVc: 21 new (denoted by an asterisk) + 1 old (reabeled according to the new naming convention) ones. Columns are the same as in Table VI. We show the period of the Schubart orbit, for the sake of comparison, and predict a new low-T orbit IVc.2.A .

Label	$T_{s.i.}$	$\frac{T_{s.i.}}{T_{Ms}}$	$\frac{T_{s.i.}}{T_{\beta}}$	$\frac{n+\bar{n}}{n_{\beta}+\bar{n}_{\beta}}$	(n, \bar{n})	Old label
IVc.0.A	4.98307	0.539429	1/10.808	1/11	0,1	Schubart
IVc.2.A	24.4804	2.65006	0.4545	5/11	2,3	?
IVc.5.A	53.8569	5.83013	1	1	5,6	moth III
IVc.12.A. α	122.532	13.2644	2.27514	2.27273	12,13	*
IVc.12.A. β	122.532	13.2644	2.27514	2.27273	12,13	*
IVc.12.B	123.675	13.3881	2.29636	2.27273	12,13	*
IVc.13.A	134.070	14.5134	2.48937	2.45455	13,14	*
IVc.15.A	153.281	16.5930	2.84608	2.81818	15,16	*
IVc.16.A	163.710	17.7220	3.03972	3	16,17	*
IVc.16.B	163.708	17.7218	3.03968	3	16,17	*
IVc.16.C	163.709	17.7219	3.03970	3	16,17	*
IVc.17.A	172.311	18.6531	3.19942	3.18182	17,18	*
IVc.17.B	173.319	18.7622	3.21814	3.18182	17,18	*
IVc.18.A	182.889	19.7982	3.39583	3.36364	18,19	*
IVc.19.A	191.207	20.6986	3.55028	3.54545	19,20	*
IVc.21.A	212.495	23.0031	3.94555	3.90909	21,22	*
IVc.22.A	222.957	24.1356	4.13980	4.09091	22,23	*
IVc.8.A	87.4850	9.47045	1.62440	1.63636	8,10	*
IVc.8.B	87.4857	9.47053	1.62441	1.63636	8,10	*
IVc.8.C	92.9007	10.0567	1.72495	1.72727	8,11	*
IVc.15.B	163.711	17.7221	3.03974	3	15,18	*
IVc.15.C	163.710	17.7220	3.03972	3	15,18	*
IVc.19.B. α	196.579	21.2801	3.65002	3.63636	19,21	*
IVc.19.B. β	196.579	21.2801	3.65002	3.63636	19,21	*

Table XXII: Non-minimal free group elements for the orbits from Table XXI – “moth III
 $(n, n + 1)$ ” sequence IVc.

Label	Free group element
IVc.0.A	ab
IVc.2.A	$(babABA)^1a(abaBAB)^1b$
IVc.5.A	$(babABA)^2a(abaBAB)^2b$
IVc.8.A	$(abaBAB)^2b(babABA)a(abaBAB)b(babABA)a(abaBAB)b(babABA)A$
IVc.8.B	$(abaBAB)^2b(babABA)a(abaBAB)b(babABA)a(abaBAB)b(babABA)A$
IVc.8.C	$(babABA)a(abaBAB)^2b(babABA)a(abaBAB)b(babABA)^2a^2$
IVc.12.A. α	$(babABA)^3A(abaBAB)^3B(babABA)^2a(abaBAB)B$
IVc.12.A. β	$(babABA)^3a(abaBAB)^3b(babABA)A(abaBAB)^2b$
IVc.12.B	$(babABA)^4b(abaBAB)^4a$
IVc.13.A	$(babABA)^2B(abaBAB)A(babABA)b(abaBAB)^2A(babABA)B(abaBAB)a$
IVc.15.A	$(babABA)^5b(abaBAB)^5a$
IVc.15.B	$(babABA)^2b(abaBAB)a(babABA)^2b(abaBAB)^2a(babABA)b(abaBAB)^2a$
IVc.15.C	$(babABA)^2b(abaBAB)a(babABA)^2b(abaBAB)^2a(babABA)b(abaBAB)^2a$
IVc.16.A	$(babABA)^2B(abaBAB)^2A(babABA)b(abaBAB)^2A(babABA)^2B(abaBAB)a$
IVc.16.B	$(babABA)^2B(abaBAB)^2A(babABA)b(abaBAB)^2A(babABA)^2B(abaBAB)a$
IVc.16.C	$(babABA)^2B(abaBAB)^2A(babABA)b(abaBAB)^2A(babABA)^2B(abaBAB)a$
IVc.17.A	$(babABA)^6A(abaBAB)^6B$
IVc.17.B	$(abaBAB)A(babABA)^2b(abaBAB)^3A(babABA)^2b(abaBAB)^3A^2$
IVc.18.A	$(babABA)^6b(abaBAB)^6a$
IVc.19.A	$(babABA)^2a(abaBAB)^2b(babABA)^3a(abaBAB)^2b(babABA)^2A(abaBAB)^3b$
IVc.19.B. α	$(babABA)^4A(abaBAB)^4B(babABA)^3A(abaBAB)^3B$
IVc.19.B. β	$(babABA)^4A(abaBAB)^4B(babABA)^3A(abaBAB)^3B$
IVc.21.A	$(babABA)^7b(abaBAB)^7a$
IVc.22.A	$(babABA)^3B(abaBAB)^2A(babABA)^2b(abaBAB)^3A(babABA)^2B(abaBAB)^2a$

8. Sequence VI – satellites of the moth I - yarn ($2n, 3n$)

Table XXIII: Orbits in the “yarn ($2n, 3n$)” sequence VI: 5 new (denoted by an asterisk) + 2 old (relabelled according to the new naming convention) ones. Columns are the same as in Table VI.

Label	$T_{\text{s.i.}}$	$\frac{T_{\text{s.i.}}}{T_{\text{Ms}}}$	$\frac{T_{\text{s.i.}}}{T_{\beta}}$	$\frac{n+\bar{n}}{n_{\beta}+\bar{n}_{\beta}}$	(n, \bar{n})	Old label
VI.2.A	24.2056	2.62031	1	1	2,3	moth I
VI.4.A	48.4115	5.24066	2.00001	2	4,6	*
VI.6.A	72.6443	7.86391	3.00114	3	6,9	yarn
VI.6.B	72.6442	7.86390	3.00113	3	6,9	*
VI.6.C	72.6443	7.86391	3.00114	3	6,9	*
VI.12.A	145.287	15.7277	6.00221	6	12,18	*
VI.14.A	169.437	18.3419	6.99991	7	14,21	*

This sequence is closely related to the “moth I ($n, n+1$)” sequence; these two together probably form a larger super-sequence (“moth I”).

These orbits have characteristic free group elements $(\text{abABaBaBAB})^n$, where $n = 1, 2, 3, \dots$, (see Table XXIV), i.e., they are topological satellites of the moth I orbit.

Orbits VI.2.A, VI.4.A and VI.6.B have reflection symmetries around two axes – the equator and the meridian that passes through the Euler point. Orbits VI.6.A, VI.6.C, VI.12.A and VI.14.A have central reflection symmetry around the Euler point.

All orbits have algebraic exchange symmetries of free group elements $(\mathbf{a}, \mathbf{A}) \leftrightarrow (\mathbf{b}, \mathbf{B})$.

Linear fit $T|E|^{3/2} = a \left(\frac{n+\bar{n}}{2} \right) + b$ for all orbits from Table XXIII gives $a = 9.6833 \pm 0.0017$ and $b = 0.009 \pm 0.017$ (see Figure 3.b in the main text).

Table XXIV: Non-minimal free group elements for the orbits from Table XXIII – satellites of the “yarn $(2n, 3n)$ ” sequence VI. Columns are the same as in Table VI.

Label	Free group element
VI.2.A	$(\mathbf{abAB})\mathbf{A}(\mathbf{baBA})\mathbf{B}$
VI.4.A	$[(\mathbf{abAB})\mathbf{A}(\mathbf{baBA})\mathbf{B}]^2$
VI.6.A	$[(\mathbf{abAB})\mathbf{A}(\mathbf{baBA})\mathbf{B}]^3$
VI.6.B	$[(\mathbf{abAB})\mathbf{A}(\mathbf{baBA})\mathbf{B}]^3$
VI.6.C	$[(\mathbf{abAB})\mathbf{A}(\mathbf{baBA})\mathbf{B}]^3$
VI.12.A	$[(\mathbf{abAB})\mathbf{A}(\mathbf{baBA})\mathbf{B}]^6$
VI.14.A	$[(\mathbf{abAB})\mathbf{A}(\mathbf{baBA})\mathbf{B}]^7$

9. Sequence VIIa – moth (n, n)

Initially, this sequence were considered jointly with the following one (VIIb) as a part of a larger sequence of orbits - sequence VII. Large deviations from the straight line and different free group element patterns suggested that sequence VII should be divided into two “smaller” sequences. Orbits were then divided into sequences VIIa and VIIb according to their topology and appearance in real space, and the resulting slopes and intercepts turned out to be significantly different, as well. These two sequences can be paired with the IVa moth I $(n, n + 1)$ and IVc moth III $(n, n + 1)$ as follows, [IVa moth I $(n, n + 1)$, VIIa moth (n, n)] and [IVc moth III $(n, n + 1)$, VIIb moth (n, n)].

Sequence VIIa orbits in real space look similar to some of the orbits from IVa sequence. Also, the IVa moth I $(n, n + 1)$ sequence and the VIIa moth (n, n) sequence are related by the change of exponent $n + 1 \rightarrow n$ in their typical free-group elements, see Tables XVI and XXVI. Thus, sequence VIIa orbits have free group elements that contain $(\mathbf{abAB})^n\mathbf{a}(\mathbf{baBA})^m\mathbf{b}$ (where n and m are integers), or products of such words. If one removes all the structures with powers n, m from $(\mathbf{abAB})^n\mathbf{a}(\mathbf{baBA})^m\mathbf{b}$, however, one obtains \mathbf{ab} , i.e., one of the topologies that can be associated with the Schubart orbit.

So, although we took the VIIb.4.A as the shortest observed (β) orbit in this sequence, we also show the period of the Schubart orbit in Table XXVII, for the sake of comparison. The

Table XXV: Orbits in the “moth (n, n) ” sequence VIIa: 8 new (denoted by an asterisk) ones. Columns are the same as in Table VI. The β orbit is taken to be VIIa.6.A. We show the period of the Schubart orbit, for the sake of comparison.

Label	$T_{\text{s.i.}}$	$\frac{T_{\text{s.i.}}}{T_{\text{M8}}}$	$\frac{T_{\text{s.i.}}}{T_{\beta}}$	$\frac{n+\bar{n}}{n_{\beta}+\bar{n}_{\beta}}$	(n, \bar{n})	Old label
VIIa.1.A	4.98307	0.520765	1/11.5848	1/12	1/2,1/2	Schubart
VIIa.2.5.A	24.9153	2.62038	0.41930	0.41667	5/2,5/2	?
VIIa.6.A	57.7280	6.24919	1	1	6,6	*
VIIa.7.A. α	67.0138	7.25440	1.16085	1.16667	7,7	*
VIIa.7.A. β	67.0138	7.25440	1.16085	1.16667	7,7	*
VIIa.10.A	94.8241	10.2649	1.64260	1.66667	10,10	*
VIIa.11.A	106.147	11.4907	1.83874	1.83333	11,11	*
VIIa.13.A	124.733	13.5026	2.16070	2.16667	13,13	*
VIIa.13.B	124.733	13.5026	2.16070	2.16667	13,13	*
VIIa.13.C	124.747	13.5041	2.16094	2.16667	13,13	*

(decent) numerical agreement suggests that the Schubart orbit might be the true progenitor of this sequence. Note, however, that Schubart is not the only possible orbit in this sequence with a period shorter than the VIIa.6.A’s: the, so far undetected, orbit VIIa.2.5.A, that has the same period as the moth I orbit, is also allowed and fits in well.

Orbits VIIa.6.A, VIIa.10.A, VIIa.11.A and VIIa.13.C, have reflection symmetries about two axes – the equator and the meridian that passes through the Euler point. Orbits VIIa.7.A. α , VIIa.7.A. β , VIIa.13.A and VIIa.13.B have central reflection symmetry about the Euler point.

For the VIIa sequence, see Table XXV, linear fit $T|E|^{3/2} = a\left(\frac{n+\bar{n}}{2}\right) + b$ gives (see Figure 3.c in the main text) $a = 9.61 \pm 0.07$ and $b = -0.2 \pm 0.7$.

Table XXVI: Non-minimal free group elements for the “moth (n, n) ” orbits from Table XXV – sequence VIIa. Columns are the same as in Table VI.

Label	Free group element
VIIa.1.A	\mathbf{aB}
VIIa.2.5.A	$(\mathbf{abAB})\mathbf{a}(\mathbf{baBA})\mathbf{B}$
VIIa.6.A	$(\mathbf{abAB})\mathbf{a}(\mathbf{baBA})\mathbf{b}(\mathbf{abAB})\mathbf{a}(\mathbf{bABA})^2\mathbf{B}$
VIIa.7.A. α	$(\mathbf{abAB})\mathbf{a}(\mathbf{baBA})^2\mathbf{b}(\mathbf{abAB})^2\mathbf{A}(\mathbf{baBA})\mathbf{B}$
VIIa.7.A. β	$(\mathbf{abAB})^2\mathbf{A}(\mathbf{baBA})\mathbf{B}(\mathbf{abAB})\mathbf{a}(\mathbf{baBA})^2\mathbf{b}$
VIIa.10.A	$(\mathbf{abAB})^3\mathbf{A}(\mathbf{baBA})^2\mathbf{B}(\mathbf{abAB})^2\mathbf{a}(\mathbf{baBA})^2\mathbf{b}$
VIIa.11.A	$[(\mathbf{baBA})\mathbf{b}(\mathbf{abAB})\mathbf{a}]^2(\mathbf{baBA})^2\mathbf{B}(\mathbf{abAB})\mathbf{A}(\mathbf{baBA})\mathbf{B}(\mathbf{abAB})\mathbf{A}$
VIIa.13.A	$(\mathbf{abAB})^2\mathbf{A}(\mathbf{baBA})^2\mathbf{B}(\mathbf{abAB})\mathbf{a}(\mathbf{baBA})\mathbf{b}$ $\times (\mathbf{abAB})^2\mathbf{A}(\mathbf{baBA})\mathbf{B}(\mathbf{abAB})\mathbf{a}(\mathbf{baBA})\mathbf{b}$
VIIa.13.B	$(\mathbf{abAB})^2\mathbf{A}(\mathbf{baBA})\mathbf{B}(\mathbf{abAB})\mathbf{a}(\mathbf{baBA})\mathbf{b}$ $\times (\mathbf{abAB})^2\mathbf{A}(\mathbf{baBA})\mathbf{B}(\mathbf{abAB})\mathbf{a}(\mathbf{baBA})^2\mathbf{b}$
VIIa.13.C	$(\mathbf{abAB})^2\mathbf{A}(\mathbf{baBA})\mathbf{B}(\mathbf{abAB})\mathbf{a}(\mathbf{baBA})^2\mathbf{B}$ $\times (\mathbf{abAB})\mathbf{a}(\mathbf{baBA})\mathbf{b}(\mathbf{abAB})^2\mathbf{A}(\mathbf{baBA})\mathbf{b}$

10. Sequence VIIb – moth (n, n)

Sequence VIIb (n, n) orbits resemble moth III $(n, n + 1)$ in real space. Also, the VIIb (n, n) orbits resemble moth III $(n, n + 1)$ sequence are related by the change of exponent $n + 1 \rightarrow n$ in their typical free-group elements, see Tables XXII and XXVIII. Thus, free group elements of sequence VIIb orbits are of the form $(\mathbf{abaBAB})^n\mathbf{b}(\mathbf{babABA})^m\mathbf{a}$ (where n and m are integers), or products of such words (see Table XXVIII). Thus, if one removes all the structures with a power from $(\mathbf{abaBAB})^2\mathbf{b}(\mathbf{babABA})\mathbf{A}$, however, one obtains \mathbf{bA} , i.e., the BHH orbits’ free group word. At the vanishing angular momentum the BHH family turns into the Schubart orbit.

So, although we took the VIIb.4.A as the β orbit, in Table XXVII we also show the period of the Schubart orbit, for the sake of comparison. The (decent) numerical agreement suggests that the Schubart orbit might be the true progenitor of this sequence. Note, however, that

Table XXVII: Orbits in the “moth (n, n) ” sequence VIIb: 12 new (denoted by an asterisk) ones. Columns are the same as in Table VI. The β orbit is taken to be VIIb.4.A. We show the period of the Schubart orbit, for the sake of comparison.

Label	$T_{s.i.}$	$\frac{T_{s.i.}}{T_{Ms}}$	$\frac{T_{s.i.}}{T_{\beta}}$	$\frac{n+\bar{n}}{n_{\beta}+\bar{n}_{\beta}}$	(n, \bar{n})	Old label
VIIb.1.A	4.98307	0.539429	1/7.8416	1/8	1/2,1/2	Schubart
VIIb.2.5.A	24.9153	2.69715	0.6376	5/8	5/2,5/2	?
VIIb.4.A	39.0752	4.22998	1	1	4,4	*
VIIb.7.A	68.6734	7.43405	1.75747	1.75	7,7	*
VIIb.7.B	68.6872	7.43555	1.75782	1.75	7,7	*
VIIb.9.A	87.4837	9.47031	2.23885	2.25	9,9	*
VIIb.10.A	98.2896	10.6401	2.51540	2.5	10,10	*
VIIb.13.A	127.900	13.8455	3.27318	3.25	13,13	*
VIIb.15.A	146.737	15.8846	3.75525	3.75	15,15	*
VIIb.15.B	146.744	15.8854	3.75543	3.75	15,15	*
VIIb.16.A	157.507	17.0505	4.03087	4	16,16	*
VIIb.17.A	168.083	18.1954	4.30153	4.25	17,17	*
VIIb.18.A	176.391	19.0947	4.51414	4.5	18,18	*
VIIb.20.A	197.691	21.4005	5.05924	5	20,20	*

Schubart is not the only possible orbit in this sequence with a period shorter than the VIIb.4.A’s: the, so far undetected, orbit VIIb.2.5.A, with (approximately) equal period as that of the moth I orbit, is also allowed.

Orbits VIIb.4.A, VIIb.7.A, VIIb.9.A, VIIb.10.A, VIIb.13.A, VIIb.15.A, VIIb.15.B, VIIb.16.A, VIIb.17.A, VIIb.18.A and VIIb.20.A have reflection symmetries about two axes – the equator and the meridian that passes through the Euler point.

Orbit VIIb.7.B has central reflection symmetry about the Euler point.

For this sequence, see Table XXVII, linear fit $T|E|^{3/2} = a\left(\frac{n+\bar{n}}{2}\right) + b$ gives (see Figure 3.d in the main text) $a = 9.88 \pm 0.04$ and $b = -0.7 \pm 0.5$

Table XXVIII: Non-minimal free group elements for the moth (n, n) orbits from Table XXVII – sequence VIIb. Columns are the same as in Table VI.

Label	Free group element
VIIb.1.A	aB
VIIb.2.5.A	$(abaBAB)bA$
VIIb.4.A	$(abaBAB)^2b(babABA)A$
VIIb.7.A	$(abaBAB)^3b(babABA)^2A$
VIIb.7.B	$(abaBAB)^2b(babABA)B(abaBAB)b(babABA)A$
VIIb.9.A	$(babABA)^2a(abaBAB)b(babABA)a(abaBAB)B$ $\times (babABA)A(abaBAB)B$
VIIb.10.A	$(babABA)^3A(abaBAB)^4b$
VIIb.11.A	$[(baBA)b(abAB)a]^2(baBA)^2B(abAB)A$ $\times (baBA)B(abAB)A$
VIIb.13.A	$(babABA)^4A(abaBAB)^5b$
VIIb.15.A	$(babABA)^2A(abaBAB)^2B(babABA)^2a(abaBAB)^2b$ $\times (babABA)^2a(abaBAB)B$
VIIb.15.B	$(babABA)^2A(abaBAB)^2B(babABA)^2a(abaBAB)^2b$ $\times (babABA)^2a(abaBAB)B$
VIIb.16.A	$(abaBAB)^6b(babABA)^5A$
VIIb.17.A	$(babABA)^6B(abaBAB)^5a$
VIIb.18.A	$(babABA)^3a(abaBAB)^2b(babABA)^2a(abaBAB)^2b$ $\times (babABA)^2A(abaBAB)^2B$
VIIb.20.A	$(babABA)^7B(abaBAB)^6a$

-
- [1] J. L. Lagrange, “Essai sur le problème des trois corps,” Oeuvres tome 6; Miscellanea Taurinensia **4**, 118–243 (1772); Oeuvres, **2**, pp. 67–121; *Mécanique Analytique*, pp. 262–286; 2nd ed. **2**, pp. 108–121; Oeuvres **12**, pp. 101–114.

- [2] Euler’s original publication is probably L. Euler, Nov. Comm. Acad. Imp. Petropolitanae, **10**, 207– 242; ibid. **11**, 152–184; Mémoires de l’Acad. de Berlin, **11**, 228–249.
- [3] M. Gascheau, Compt. Rend. 16, 393-394 (1843).
- [4] E. J. Routh, Proc. Lond. Math. Soc. 6, 86-97 (1875).
- [5] J. Schubart, Astron. Nachr. **283**, 17 (1956).
- [6] M. Hénon, Celest. Mech. **13**, 267 (1976).
- [7] M. Hénon, Celest. Mech. **15**, 243 (1977).
- [8] R. Broucke and D. Boggs, Celest. Mech. **11**, 13 (1975).
- [9] R. Broucke, Celest. Mech. **12**, 439 (1975).
- [10] J.D. Hadjidemetriou, Celest. Mech. **12**, 155 (1975).
- [11] J.D. Hadjidemetriou and Th. Christides, Celest. Mech. **12**, 175 (1975).
- [12] J.D. Hadjidemetriou, Celest. Mech. **12**, 255 (1975).
- [13] R. Broucke, Astron. Astrophys. **73**, 303 (1979).
- [14] E. Davoust, and R. Broucke, Astron. Astrophys. **112**, 305-320 (1982).
- [15] E. Strömberg, Bull. Astron., Paris 9, 87 (1933).
- [16] C. Moore, Phys. Rev. Lett. **70**, 3675–3679 (1993).
- [17] A. Chenciner and R. Montgomery, Ann. Math. **152**, 881–901 (2000).
- [18] C. Simó, p. 209 - 228 in *Celestial Mechanics* (dedicated to Donald Saari, Evanston, IL, 1999), Edited by, Alain Chenciner, Richard Cushman, Clark Robinson, and Zhihong Jeff Xia. Contemporary Mathematics, Vol 292, AMS, Providence, R.I., (2002).
- [19] J. Galán, F. J. Muñoz-Almaraz, E. Freire, E. Doedel, and A. Vanderbauwhede, Phys. Rev. Lett. **88**, 241101 (2002).
- [20] M. Šuvakov, and V. Dmitrašinović, Phys. Rev. Lett. **110**, 114301 (2013).
- [21] M. Šuvakov, Celest. Mech. Dyn. Astron. **119**, 369-377 (2014).
- [22] A. I. Martynova, V. V. Orlov, and A. V. Rubinov, Astron. Rep. **53**, 710 (2009).
- [23] P. P. Iasko and V. V. Orlov, Astron. Rep. **58**, 869-879. (2014).
- [24] M. Šuvakov and M. Shibayama, Celest. Mech. Dyn. Astron. **124**, 155-162 (2016).
- [25] <http://three-body.ipb.ac.rs/> and <http://three-body.ipb.ac.rs/sequences.php>
- [26] V. Dmitrašinović and M. Šuvakov, Phys. Lett. **A 379**, 1939-1945 (2015).
- [27] M. R. Janković and V. Dmitrašinović, Phys. Rev. Lett. **116**, 064301(5) (2016).
- [28] G. D. Birkhoff and D. C. Lewis, Ann. di Mat. (4) **12**, 117-133 (1933).

- [29] M. Šuvakov, and V. Dmitrašinović, *Am. J. Phys.* **82**, 609-619 (2014).
- [30] Erwin Fehlberg, NASA Technical Report 315 (1969) (unpublished). See also *Computing (Arch. Elektron. Rechnen)* **6**, 61–71 (1970).
- [31] Ernst Hairer, Syvert Nørsett, and Gerhard Wanner, *Solving Ordinary Differential Equations I: Nonstiff Problems*, 2nd ed. (Springer-Verlag, Berlin, 1993), Chap. II.5.
- [32] Carl Gustav Jacob Jacobi, *Vorlesungen über Dynamik, Gesammelte Werke*, Vol. VIII, Supplement (1884); reprinted by (Chelsea Publishing Company, New York, 1969), pp. 221–231.
- [33] T. Iwai, “A geometric setting for internal motions of the quantum three-body system,” *J. Math. Phys.* **28**, 964, 1315–1326 (1987).
- [34] R. Montgomery, *Nonlinearity* **11**, 363 - 376 (1998).
- [35] R. Moeckel and R. Montgomery, arXiv:1412.2263 (math.DS).
- [36] L. D. Landau and E. M. Lifshitz, *Mechanics*, 3rd ed. (Butterworth-Heinemann, Oxford, 1976), Sec. 10.
- [37] R. Montgomery, *Ergodic Theory and Dynamical Systems* **27** (6), 1933–1946 (2007).
- [38] Ana Hudomal, “New Periodic Solutions to the Three-Body Problem and Gravitational Waves”, Master of Science thesis at the Faculty of Physics, Belgrade University, October 2015.
- [39] W. Klingenberg, *Lectures on Closed Geodesics*, Springer-Verlag Berlin Heidelberg New York (1978).
- [40] K. Richter, G. Tanner and D. Wintgen, *Phys. Rev. A* **48**, 4182 (1993).
- [41] G. D. Birkhoff, *Mem. Pon. Acad. Sci. Novi Lyncaei* (3) 1, 85-216 (1935).
- [42] C. L. Siegel and J. K. Moser, *Lectures on Celestial Mechanics*, Springer-Verlag Berlin Heidelberg (1971).
- [43] J. K. Moser and E. J. Zehnder, *Notes on Dynamical Systems*, American Mathematical Society, Providence R. I. (2000).
- [44] K. Zare and S. Chesley, *Chaos*, **8**, No. 2, 475 (1998).
- [45] Z. E. Musielak, and B. Quarles, “The three-body problem”, *Rep. Prog. Phys.* **77**, 065901 (2014).
- [46] A. Tokovinin, “Dynamics of Multiple Stars: Observations”, pp. 615-619 in *Massive Stars in Interacting Binaries*, ASP Conference Series, Vol. 367, editors N. St-Louis & A.F.J. Moffat (2007).

- [47] S. M. Ransom *et al.*, Nature **505**, 520 (2014)
- [48] V. Dmitrašinić, Milovan Šuvakov, and Ana Hudomal, Phys. Rev. Lett. **113**, 101102 (2014)
- [49] T. Chiba, T. Imai and H. Asada, Mon. Not. Roy. Astron. Soc. **377**, 269 (2007)
- [50] Y. Torigoe, K. Hattori and H. Asada, Phys. Rev. Lett. **102**, 251101 (2009)
- [51] H. Asada, Phys. Rev. D **80**, 064021 (2009)
- [52] P. Galaviz and B. Bruegmann, Phys. Rev. D **83**, 084013 (2011)
- [53] B. P. Abbott *et al.* Phys. Rev. Lett. **116**, no. 6, 061102 (2016)
- [54] B. P. Abbott *et al.* Phys. Rev. Lett. **116**, no. 24, 241103 (2016)
- [55] B. P. Abbott *et al.* Phys. Rev. X **6**, no. 4, 041015 (2016)
- [56] Kedron Silsbee and Scott Tremaine, arXiv:1608.07642 [astro-ph.HE]
- [57] R. P. Feynman, “*Feynman’s Lost Lecture: The Motion of Planets Around the Sun*”, edited by D. L. Goodstein and J. R. Goodstein, W - W. Norton & Company, New York London (1999).
- [58] Tomoyuki Yamamoto and Kunihiro Kaneko, Phys. Rev. Lett. **70**, 1928 (1993).
- [59] Danya Rose, University of Sydney Ph.D. thesis “Geometric phase and periodic orbits of the equal-mass, planar three-body problem with vanishing angular momentum” (2016). Available at <https://ses.library.usyd.edu.au/handle/2123/14416>
- [60] Xiaoming Li and Shijun Liao, “One hundred and fifty-two new families of Newtonian periodic planar three-body orbits”, unpublished (2017); arXiv: 1705.00527.
- [61] Though several orbits had been rediscovered, most notably by Moore [16].
- [62] syzygies are collinear configurations, or points on the equator of the shape sphere.
- [63] This is only possible for periodic orbits that form closed loops on the shape sphere; otherwise one would have to define one symbol for crossing the equator from above and another one for crossing from below.
- [64] Eq. (5) is manifestly a special case of Eq. (6).
- [65] Here, by “minimal total number of letters” we mean the number of letters after all pairs of adjacent identical small and capital letters, such as **aA**, have been eliminated
- [66] In Ref. [24], it was conjectured that the topological-power satellites of the figure-eight orbit are a consequence of the Poincaré-Birkhoff theorem, Ref. [41], see also §24 in Ref. [42] and §2.7 in Ref. [43], as applied to the figure-8 orbit. That conjecture is incorrect, however, because the Poincaré-Birkhoff theorem applies only to systems with two degrees-of-freedom (d.o.f.), to which class the planar three-body problem does not belong.

- [67] A possible explanation for the existence of this discrepancy lies in the presence of a new parameter, set by the non-vanishing angular momentum, that does not exist in orbits with vanishing angular momentum.
- [68] Several such periodic orbits have been found in Refs. [40, 58], but their topological classification was not considered.